Nanoscale Advances

ROYAL SOCIETY OF CHEMISTRY

PAPER

View Article Online
View Journal | View Issue

Cite this: *Nanoscale Adv.*, 2025, **7**, 2528

Green procedures for synthesizing potential *h*NMDA receptor allosteric modulators through reduction and one-pot reductive acetylation of nitro(hetero)arenes using a superparamagnetic Fe_3O_4@APTMS@Cp_2ZrCl_x (x = 0, 1, 2) nanocatalyst†

Hossein Mousavi,* Behzad Zeynizadeh and Farhad Sepehraddin

Received 25th October 2024
Accepted 3rd February 2025

DOI: 10.1039/d4na00882k

rsc.li/nanoscale-advances

The conversion of nitro(hetero)arenes to corresponding (hetero)aryl amines and other practical organic compounds plays a crucial role in various sciences, especially environmental remediation and public health. In the current research work, diverse green and efficient strategies for the convenient reduction (hydrogenation) and one-pot two-step reductive acetylation of nitro(hetero)arenes using a core–shell-type mesoporous zirconocene-containing magnetically recoverable nanocomposite (*viz.* Fe_3O_4@APTMS@Cp_2ZrCl_x (x = 0, 1, 2)) as a powerful nanocatalytic system have been developed. In the presented organic transformations, the superparamagnetic Fe_3O_4@APTMS@Cp_2ZrCl_x (x = 0, 1, 2) nanocomposite exhibited satisfactory turnover numbers (TONs) and turnover frequencies (TOFs), along with acceptable reusability. On the other hand, we investigated the potential biological effect of the synthesized (hetero)aryl amines and *N*-(hetero)aryl acetamides against the transmembrane domain (TMD) of the human *N*-methyl-D-aspartate (*h*NMDA) receptor based on molecular docking studies. Furthermore, the drug-likeness properties of our hit compound (*viz.* *N*-(3-(1-hydroxyethyl)phenyl) acetamide) have been scrutinized by *in silico* ADMET analyses.

1. Introduction

Numerous (hetero)aromatic nitro compounds are toxic and hazardous.[1] Therefore, exploring green, efficient, economical, and simple synthetic strategies for conversion of the mentioned nitro-containing compounds to the corresponding (hetero)aryl amines and/or other valuable organic compounds, including *N*-(hetero)aryl acetamides, is of great significance for environmental remediation, public health, and also medicinal chemistry (Fig. 1).[2]

In the new century, "*Green Chemistry*" has become one of the hottest and most significant terms in all branches of chemistry.[3] Based on green chemistry principles, designing effective, eco-friendly, recoverable, and reusable heterogeneous catalytic systems is still an ultimate goal for numerous critical organic transformations. During the last three decades, zirconium (Zr)-containing catalytic systems have played an essential role in organic synthesis.[4] It is worth noting that zirconium is one of the earth-abundant transition metals (EATMs),[5] and also based on a paper, which was reported by Bystrzanowska, Petkov, and Tobiszewski in 2019, results of the multicriteria decision analysis (MCDA) approach demonstrated that Zr-containing heterogeneous catalytic systems are environmentally desirable compared to rhodium (Rh)-, copper (Cu)-, cadmium (Cd)-, palladium (Pd)-, gold (Au)-, cobalt (Co)-, and also nickel (Ni)-based systems.[6] On the other hand, the recoverability and reusability of the catalyst are crucial factors from the green chemistry point of view. In this regard, one of the best choices is the use of magnetic nanoparticles (such as Fe_3O_4, $CuFe_2O_4$, $ZrFe_2O_4$, $MgFe_2O_4$, $CoFe_2O_4$, $NiFe_2O_4$, $MnFe_2O_4$, *etc.*) as a core part of a core–shell-type catalytic system.[7] In addition to the catalyst, according to the principles of green chemistry, the solvent is another main factor in organic synthesis. Undoubtedly, water is the most preferable choice compared to all common solvents because of its unique features, such as abundance, non-toxicity, sustainability, *etc.*[8]

Neurodegenerative diseases (NDs) are among the alarming and significant health challenges facing contemporary society.[9] In a situation where most of them are still incurable, many endeavors have been made to overcome or control them. *N*-methyl-D-aspartate (NMDA) receptors, known as ionotropic glutamate-gated cation channels with high calcium (Ca^{II}) permeability, are members of the immense family of glutamate receptors and are linked to synapse development, synaptic plasticity, and cognitive functions, which are vital for

Department of Organic Chemistry, Faculty of Chemistry, Urmia University, Urmia, Iran. E-mail: 1hossein.mousavi@gmail.com

† Electronic supplementary information (ESI) available. See DOI: https://doi.org/10.1039/d4na00882k

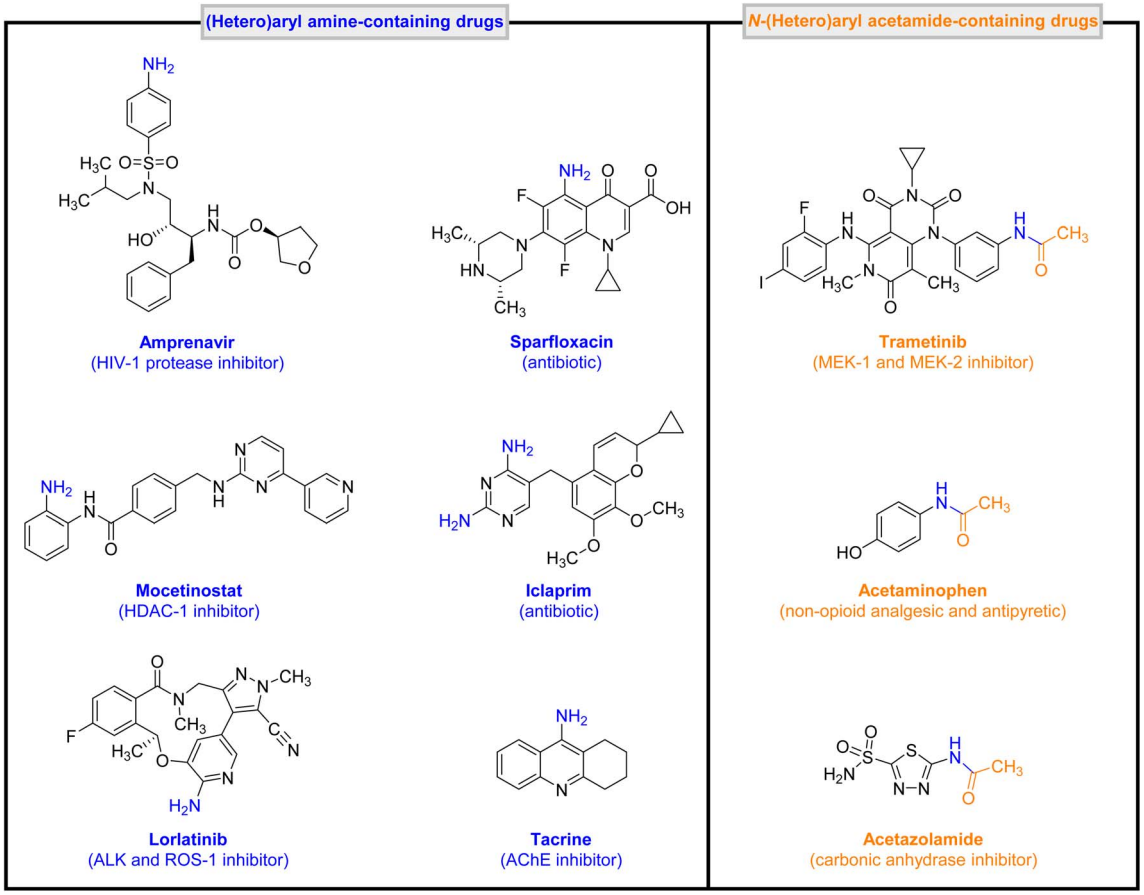

Fig. 1 Representative examples of drugs bearing (hetero)aryl amine and *N*-(hetero)aryl acetamide.

diverse aspects of brain function. Notably, research has highlighted the significance of NMDA receptors in various NDs (such as Alzheimer's disease (AD), Parkinson's disease (PD), and Huntington's disease (HD)) and neuro-developmental disorders including intellectual disability, schizophrenia, autism, and epilepsy.[10,11] Also, NMDA receptors have a confirmed role in ischemic brain injury and neuropathic pain.[11]

In recent years, the computer-aided drug design (CADD) strategy has been recognized as a powerful approach that utilizes particular computational methods and algorithms to speed up and enhance the drug discovery and development process and helps researchers by identifying and validating potential drug targets *via* analyzing biological data and understanding the interactions between proteins, enzymes, receptors, and many other molecules concerned in disease pathways.[12]

In continuation of our research on various types of catalytic organic transformations[13–16] and also due to the importance of introducing a new environmentally benign approach to the conversion of nitro(hetero)arenes to valuable organic compounds, herein we wish to report diverse green and efficient strategies for the convenient reduction (hydrogenation) and one-pot two-step reductive acetylation of nitro(hetero)arenes using a superparamagnetic Fe_3O_4@APTMS@Cp_2ZrCl_x (x = 0, 1, 2) nanocomposite as an efficient core–shell-type mesoporous zirconocene-containing recoverable nanocatalyst (Fig. 2). Besides, we have investigated the potential medicinal effect of all synthesized (hetero)aryl amines and *N*-(hetero)aryl acetamides against the transmembrane domain (TMD) of the human *N*-methyl-D-aspartate (*h*NMDA) receptor using molecular docking studies. We have also examined the drug-likeness properties of our hit compound (*viz.* *N*-(3-(1-hydroxyethyl) phenyl)acetamide) through *in silico* ADMET analyses.

2. Results and discussion

2.1. Preparation of the superparamagnetic core–shell-type Fe_3O_4@APTMS@Cp_2ZrCl_x (x = 0, 1, 2) nanocomposite

We started our work by preparing the superparamagnetic Fe_3O_4@APTMS@Cp_2ZrCl_x (x = 0, 1, 2) nanocomposite according to our previously published papers (Fig. 3).[14–16] It is worthwhile to note that the structure of the mentioned core–shell-type magnetic system was characterized by Fourier transform infrared (FT-IR) spectroscopy, powder X-ray diffraction (PXRD), scanning electron microscopy (SEM), SEM-based energy-dispersive X-ray (EDX) spectroscopy, inductively coupled plasma-optical emission spectrometry (ICP-OES), alternating gradient force magnetometry (AGFM), thermogravimetric

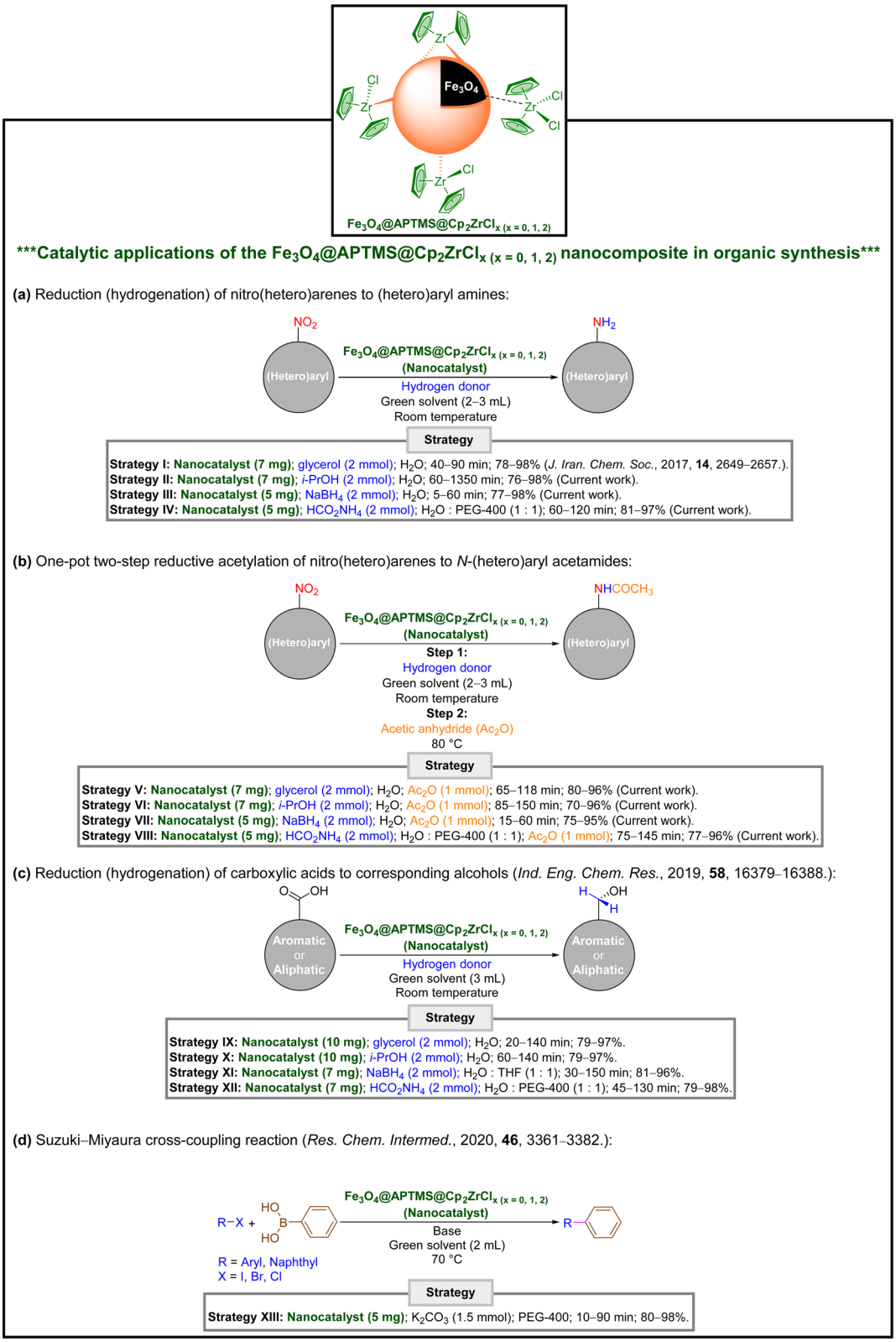

Fig. 2 Catalytic applications of the as-prepared Fe_3O_4@APTMS@Cp_2ZrCl_x (x = 0, 1, 2) nanocomposite.

analysis (TGA), and nitrogen (N_2) gas adsorption–desorption analysis (Fig. 4), which was reported and discussed in our previously published papers.[14–16]

In the FT-IR spectra of the as-prepared Fe_3O_4@APTMS@Cp_2ZrCl_x (x = 0, 1, 2) nanocomposite (Fig. 4, section a), the broad peak in the region of 3500 cm^{-1} to 3000 cm^{-1} is

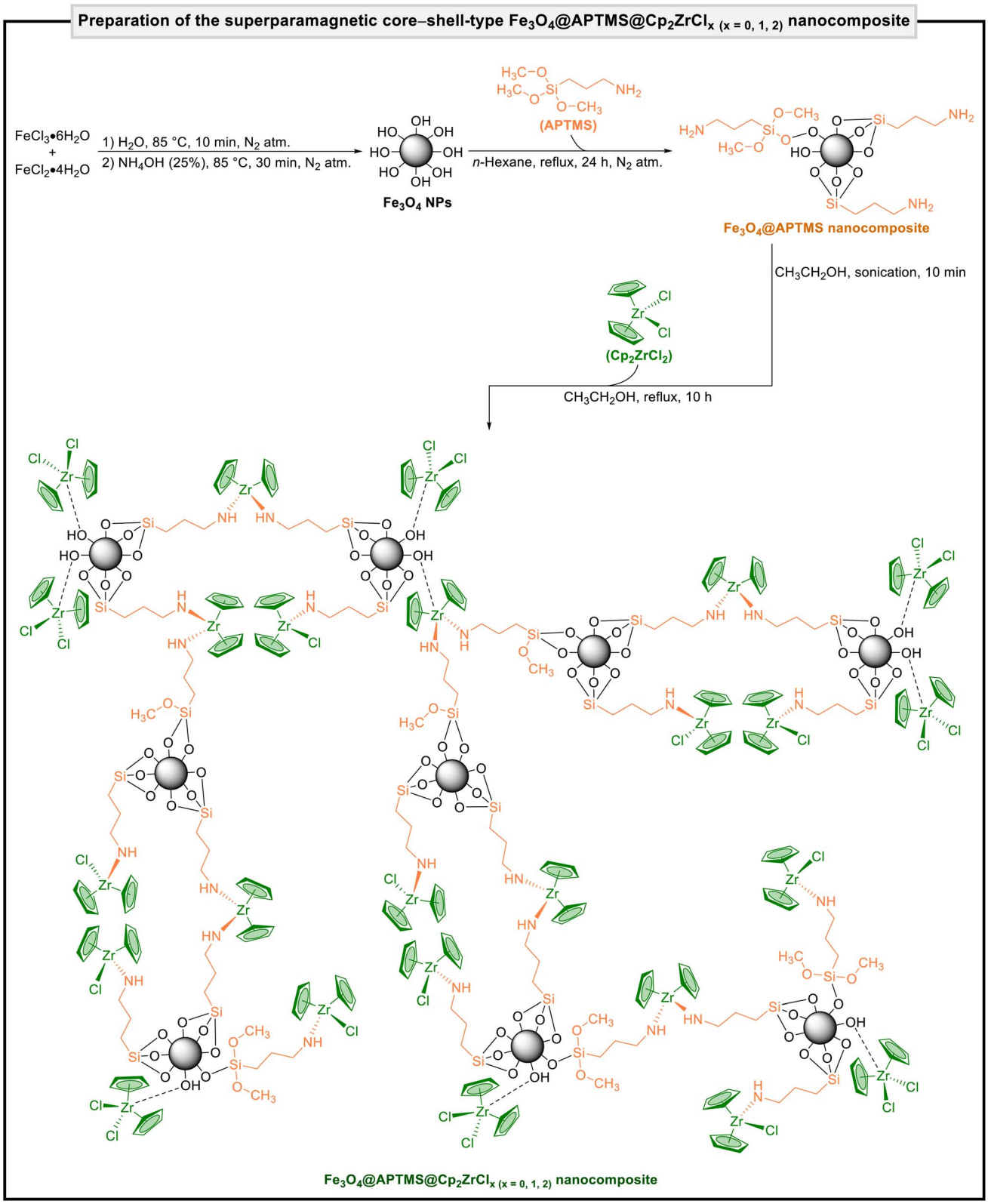

Fig. 3 Preparation of the superparamagnetic core–shell-type Fe_3O_4@APTMS@Cp_2ZrCl_x (x = 0, 1, 2) nanocomposite.

related to the free hydroxyl and stretching vibration of amine functional groups. Additionally, the three peaks at 2958 cm^{-1}, 2925 cm^{-1}, and 2851 cm^{-1} correspond to the C–H stretching vibrations of the existing –CH (aromatic), $–CH_2–$, and $–CH_3$ (in $Si–O–CH_3$) functional groups. The strong absorption peak at 1621 cm^{-1} is associated with the bending vibration of free H_2O

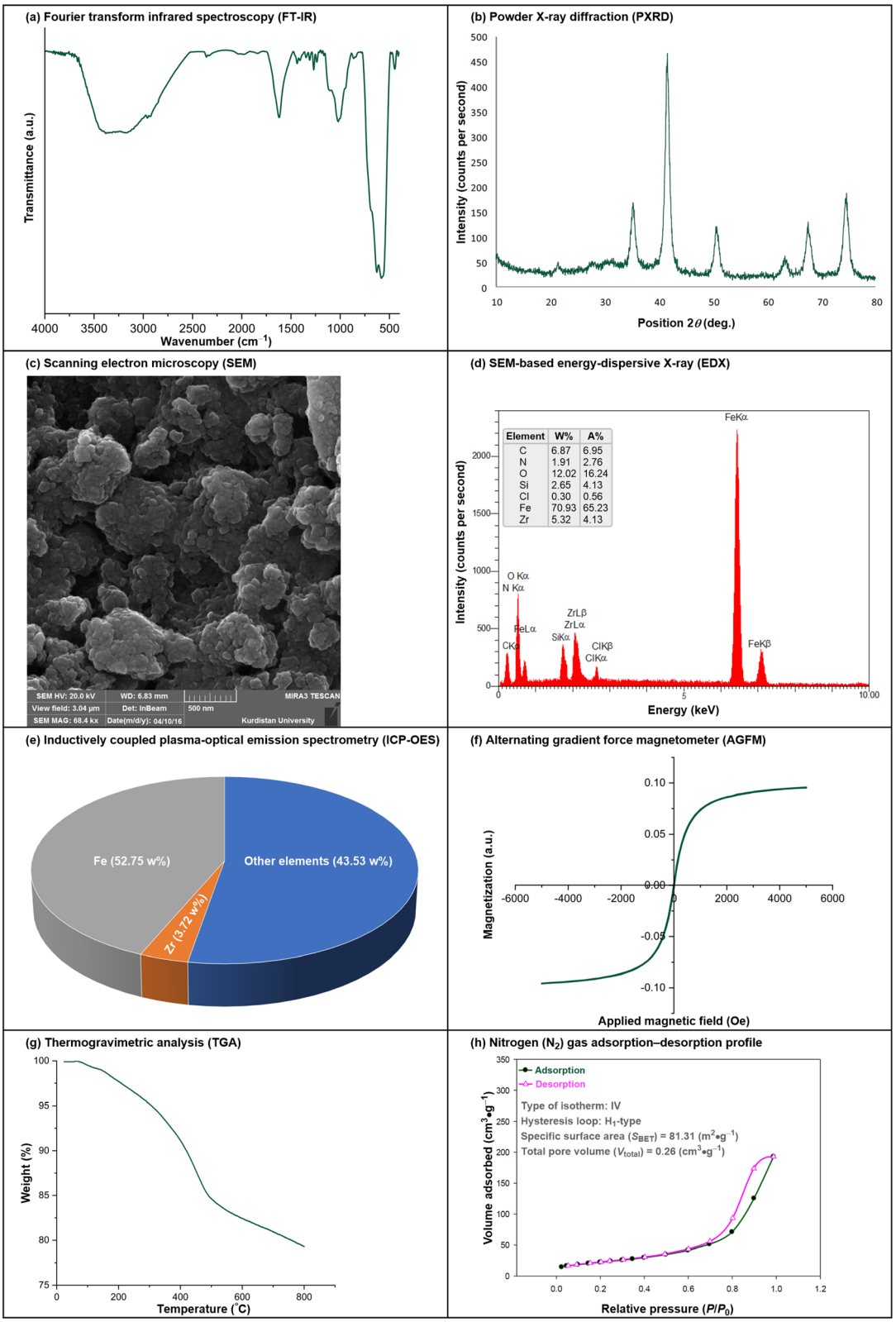

Fig. 4 Characterization analyses of the Fe_3O_4@APTMS@Cp_2ZrCl_x (x = 0, 1, 2) nanocomposite.

that adsorbed on the surface of Fe_3O_4 nanoparticles, the C=C stretching vibration of the cyclopentadienyl (Cp) ligand, and N–H bending vibrations, which overlapped in one peak. Also, the two peaks at 1437 cm^{-1} and 1407 cm^{-1} can be related to the C–O (stretching), scissoring mode of the $-CH_2-$ groups (bending), and stretching vibration of Si–CH_2. Notably,

Table 1 Green and convenient reduction (hydrogenation) of nitro(hetero)arenes to the corresponding (hetero)aryl amines catalyzed by the Fe_3O_4@APTMS@$Cp_2ZrCl_{x\ (x\ =\ 0,\ 1,\ 2)}$ nanocomposite[a]

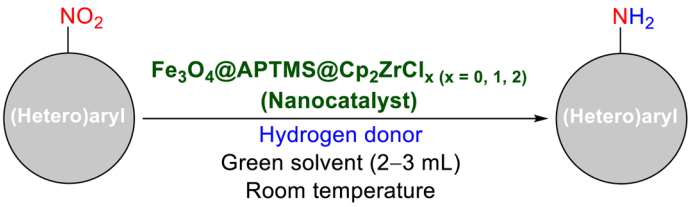

Strategy

Strategy I: **Nanocatalyst (7 mg)**; glycerol (2 mmol); H_2O; 40–90 min; 78–98% (*J. Iran. Chem. Soc.*, 2017, **14**, 2649–2657.).
Strategy II: **Nanocatalyst (7 mg)**; *i*-PrOH (2 mmol); H_2O; 60–1350 min; 76–98% (Current work).
Strategy III: **Nanocatalyst (5 mg)**; $NaBH_4$ (2 mmol); H_2O; 5–60 min; 77–98% (Current work).
Strategy IV: **Nanocatalyst (5 mg)**; HCO_2NH_4 (2 mmol); H_2O : PEG-400 (1 : 1); 60–120 min; 81–97% (Current work).

			Strategy			
Entry	Substrate	Product	Strategy I	Strategy II	Strategy III	Strategy IV
1	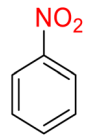	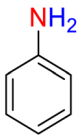	Time = 40 min Yield = 96% TON = 336.84 TOF = 8.42	Time = 60 min Yield = 97% TON = 340.35 TOF = 5.67	Time = 10 min Yield = 95% TON = 467.98 TOF = 46.80	Time = 60 min Yield = 97% TON = 477.83 TOF = 7.96
2	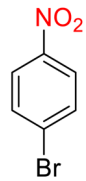	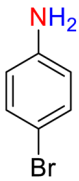	Time = 60 min Yield = 98% TON = 343.86 TOF = 5.73	Time = 75 min Yield = 93% TON = 326.31 TOF = 4.35	Time = 10 min Yield = 97% TON = 477.83 TOF = 47.78	Time = 60 min Yield = 90% TON = 443.35 TOF = 7.39
3	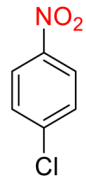	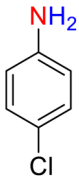	Time = 55 min Yield = 96% TON = 336.84 TOF = 6.12	Time = 100 min Yield = 90% TON = 315.79 TOF = 3.16	Time = 15 min Yield = 95% TON = 467.98 TOF = 31.20	Time = 75 min Yield = 89% TON = 438.42 TOF = 5.84
4	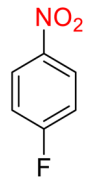	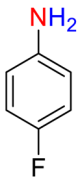	Time = 50 min Yield = 91% TON = 319.30 TOF = 6.38	Time = 60 min Yield = 98% TON = 343.86 TOF = 5.73	Time = 5 min Yield = 98% TON = 482.76 TOF = 96.55	Time = 60 min Yield = 95% TON = 467.98 TOF = 7.80
5	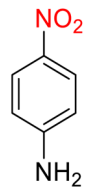	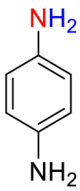	Time = 50 min Yield = 95% TON = 333.33 TOF = 6.67	Time = 80 min Yield = 84% TON = 294.73 TOF = 3.68	Time = 10 min Yield = 93% TON = 458.13 TOF = 45.81	Time = 70 min Yield = 90% TON = 443.35 TOF = 6.33
6	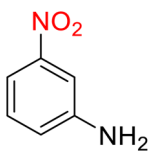	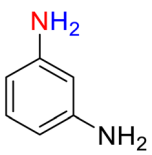	Time = 60 min Yield = 90% TON = 315.79 TOF = 5.26	Time = 120 min Yield = 82% TON = 287.72 TOF = 2.40	Time = 15 min Yield = 93% TON = 458.13 TOF = 30.54	Time = 90 min Yield = 87% TON = 443.35 TOF = 4.93
7		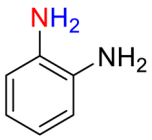	Time = 85 min Yield = 85% TON = 298.24 TOF = 3.51	Time = 120 min Yield = 78% TON = 273.68 TOF = 2.28	Time = 20 min Yield = 90% TON = 443.35 TOF = 22.17	Time = 120 min Yield = 81% TON = 399.01 TOF = 3.32

Table 1 (*Contd.*)

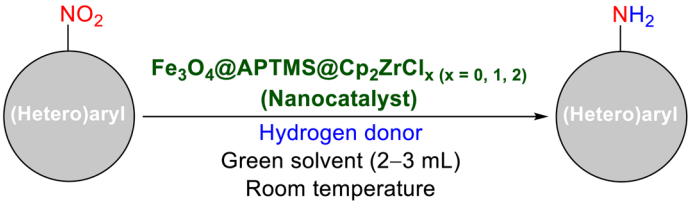

Strategy

Strategy I: **Nanocatalyst (7 mg)**; glycerol (2 mmol); H_2O; 40–90 min; 78–98% (*J. Iran. Chem. Soc.*, 2017, **14**, 2649–2657.).
Strategy II: **Nanocatalyst (7 mg)**; *i*-PrOH (2 mmol); H_2O; 60–1350 min; 76–98% (Current work).
Strategy III: **Nanocatalyst (5 mg)**; $NaBH_4$ (2 mmol); H_2O; 5–60 min; 77–98% (Current work).
Strategy IV: **Nanocatalyst (5 mg)**; HCO_2NH_4 (2 mmol); H_2O : PEG-400 (1 : 1); 60–120 min; 81–97% (Current work).

			Strategy			
Entry	Substrate	Product	Strategy I	Strategy II	Strategy III	Strategy IV
8	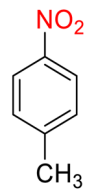	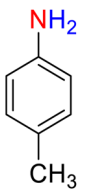	Time = 45 min Yield = 93% TON = 326.31 TOF = 7.25	Time = 70 min Yield = 89% TON = 312.28 TOF = 4.46	Time = 15 min Yield = 94% TON = 463.05 TOF = 30.87	Time = 70 min Yield = 93% TON = 458.13 TOF = 6.54
9	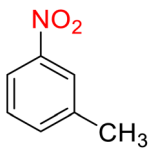	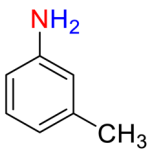	Time = 45 min Yield = 87% TON = 305.26 TOF = 6.78	Time = 100 min Yield = 89% TON = 312.28 TOF = 3.12	Time = 20 min Yield = 93% TON = 458.13 TOF = 22.91	Time = 80 min Yield = 87% TON = 428.57 TOF = 5.36
10		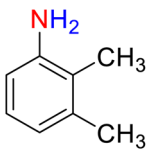	Time = 90 min Yield = 95% TON = 333.33 TOF = 3.70	Time = 120 min Yield = 84% TON = 294.74 TOF = 2.46	Time = 20 min Yield = 90% TON = 443.35 TOF = 22.17	Time = 100 min Yield = 89% TON = 438.42 TOF = 4.38
11	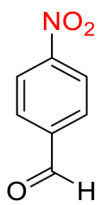	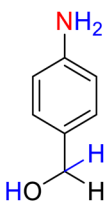	Time = 60 min Yield = 88% TON = 308.77 TOF = 5.15	Time = 120 min Yield = 88% TON = 308.77 TOF = 2.57	Time = 30 min Yield = 86% TON = 423.64 TOF = 14.12	Time = 85 min Yield = 86% TON = 423.64 TOF = 4.98
12	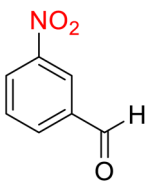	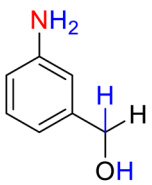	Time = 60 min Yield = 90% TON = 315.79 TOF = 5.26	Time = 120 min Yield = 81% TON = 284.21 TOF = 2.37	Time = 35 min Yield = 84% TON = 413.79 TOF = 11.82	Time = 120 min Yield = 85% TON = 418.72 TOF = 3.49
13	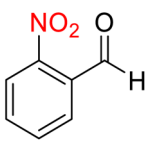	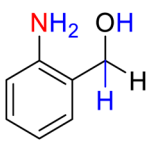	Time = 75 min Yield = 90% TON = 315.79 TOF = 4.21	Time = 120 min Yield = 76% TON = 266.67 TOF = 2.22	Time = 40 min Yield = 77% TON = 379.31 TOF = 9.48	Time = 120 min Yield = 81% TON = 399.01 TOF = 3.32
14	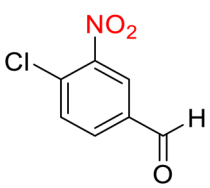	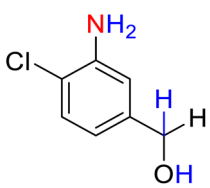	Time = 65 min Yield = 78% TON = 273.68 TOF = 4.21	Time = 120 min Yield = 84% TON = 294.74 TOF = 2.46	Time = 40 min Yield = 81% TON = 399.01 TOF = 9.97	Time = 85 min Yield = 87% TON = 428.57 TOF = 5.04

Table 1 (*Contd.*)

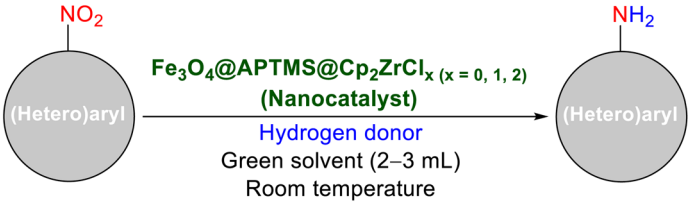

Strategy

Strategy I: **Nanocatalyst (7 mg)**; glycerol (2 mmol); H_2O; 40–90 min; 78–98% (*J. Iran. Chem. Soc.*, 2017, **14**, 2649–2657.).
Strategy II: **Nanocatalyst (7 mg)**; *i*-PrOH (2 mmol); H_2O; 60–1350 min; 76–98% (Current work).
Strategy III: **Nanocatalyst (5 mg)**; $NaBH_4$ (2 mmol); H_2O; 5–60 min; 77–98% (Current work).
Strategy IV: **Nanocatalyst (5 mg)**; HCO_2NH_4 (2 mmol); H_2O : PEG-400 (1 : 1); 60–120 min; 81–97% (Current work).

			Strategy			
Entry	Substrate	Product	Strategy I	Strategy II	Strategy III	Strategy IV
15	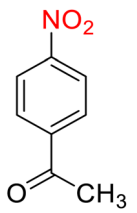	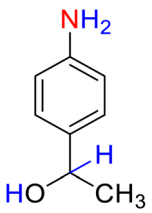	Time = 40 min Yield = 87% TON = 305.26 TOF = 7.63	Time = 85 min Yield = 87% TON = 305.26 TOF = 3.59	Time = 30 min Yield = 86% TON = 423.64 TOF = 14.12	Time = 90 min Yield = 89% TON = 438.42 TOF = 4.87
16	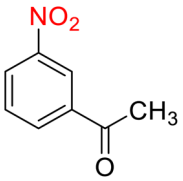	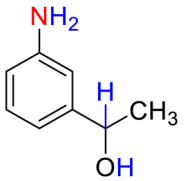	Time = 40 min Yield = 92% TON = 322.81 TOF = 8.07	Time = 100 min Yield = 88% TON = 308.77 TOF = 3.09	Time = 30 min Yield = 82% TON = 403.94 TOF = 13.46	Time = 90 min Yield = 85% TON = 418.72 TOF = 4.65
17		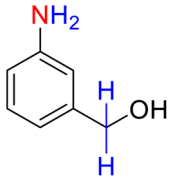	Time = 90 min Yield = 95% TON = 333.33 TOF = 3.70	Time = 135 min Yield = 89% TON = 312.28 TOF = 2.31	Time = 60 min Yield = 80% TON = 394.09 TOF = 6.57	Time = 120 min Yield = 90% TON = 443.35 TOF = 3.69
18	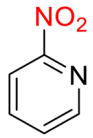	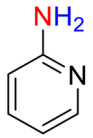	Time = 65 min Yield = 88% TON = 308.77 TOF = 4.75	Time = 75 min Yield = 90% TON = 315.79 TOF = 4.21	Time = 25 min Yield = 87% TON = 428.57 TOF = 17.14	Time = 60 min Yield = 91% TON = 448.27 TOF = 7.47

[a] (a) The strategy I (except entries 4 and 17) was reported in ref. 14. (b) TON (turnover number) = [(mol of product formed)/(mol of catalyst used)]. (c) TOF (turnover frequency) = [(mol of product formed)/(mol of catalyst used) × (time)]. (d) The TON and TOF values were calculated based on the existing amount of zirconium (Zr) in the structure of the as-prepared Fe_3O_4@APTMS@Cp_2ZrCl_x $_{(x\ =\ 0,\ 1,\ 2)}$ nanocomposite based on ICP-OES analysis.

the region from 1345 cm^{-1} to 1212 cm^{-1} can be related to stretching vibrations of C–N and C–O, as well as out-of-plane wagging and twisting bending vibrations of the –CH_2– groups along with the bending vibration of Si–CH_2. The two relatively weak peaks at 1188 cm^{-1} and 1164 cm^{-1}, along with the strong peak at 1097 cm^{-1}, can correspond to Si–OCH_3. The peaks at 1020 cm^{-1}, 998 cm^{-1}, 945 cm^{-1}, 863 cm^{-1}, and 838 cm^{-1} are related to the out-of-plane bending vibrations of the aromatic C–H bonds belonging to the structure of the cyclopentadienyl (Cp) ligand. The peak attributed to the in-plane rocking-type bending vibrations of the –CH_2– groups appears at 690 cm^{-1}. Furthermore, the three strong peaks at 628 cm^{-1}, 581 cm^{-1}, and 564 cm^{-1} are associated with the splitting ν_1 vibration of Fe^{2+}–O^{2-}, while the peak at 446 cm^{-1} belongs to the splitting ν_2 vibration of Fe^{3+}–O^{2-}.

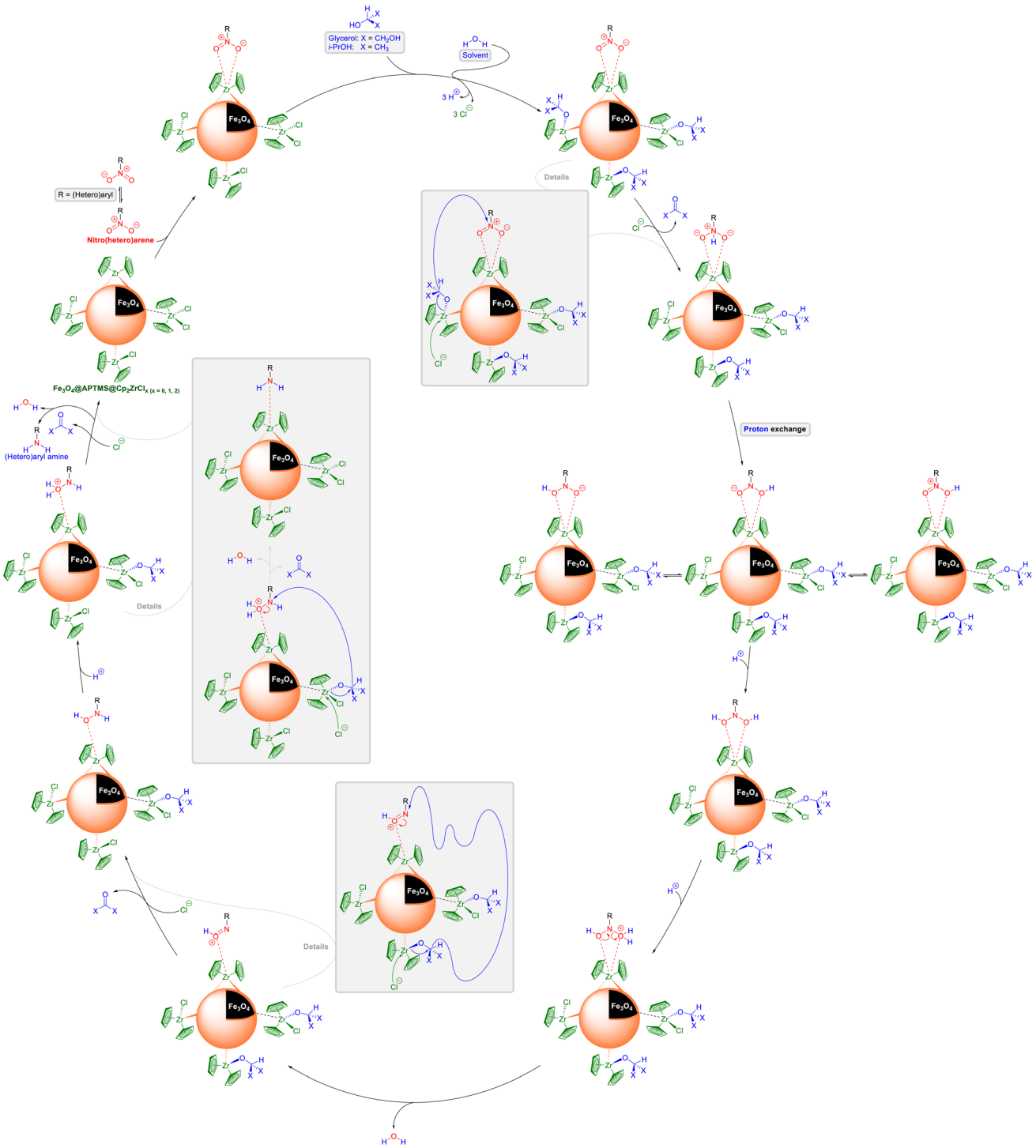

Scheme 1 Proposed mechanism for the reduction (hydrogenation) of nitro(hetero)arenes to the corresponding (hetero)aryl amines using glycerol or *i*-PrOH catalyzed by the Fe_3O_4@APTMS@Cp_2ZrCl_x (x = 0, 1, 2) nanocomposite through the direct hydrogen transfer pathway.

The PXRD plot of the as-prepared Fe_3O_4@APTMS@Cp_2-$ZrCl_x$ (x = 0, 1, 2) nanocomposite is presented in Fig. 4 (section b). In addition to the peaks corresponding to the Fe_3O_4 NPs, some distinct PXRD peaks related to silicon (Si) appeared at $2\theta = 27.69°$ (broad), 68.87°, and 76.67°. Furthermore, the peak at $2\theta = 22.13°$, associated with the (002) lattice spacing of carbon-based materials with an amorphous nature, may correspond to the Cp ligand and aliphatic chains. Notably, several distinct PXRD planes of zirconium (Zr), including (100), (002), (101), (103), (200), (201), (004), and (202), overlap with the peaks of Fe_3O_4 NPs and Si.

The scanning electron microscopy (SEM) image of the as-prepared Fe_3O_4@APTMS@Cp_2ZrCl_x (x = 0, 1, 2) nanocomposite (Fig. 4, section c) shows the morphology and size distribution of the particles. Also, the SEM-based energy-dispersive X-ray (EDX)

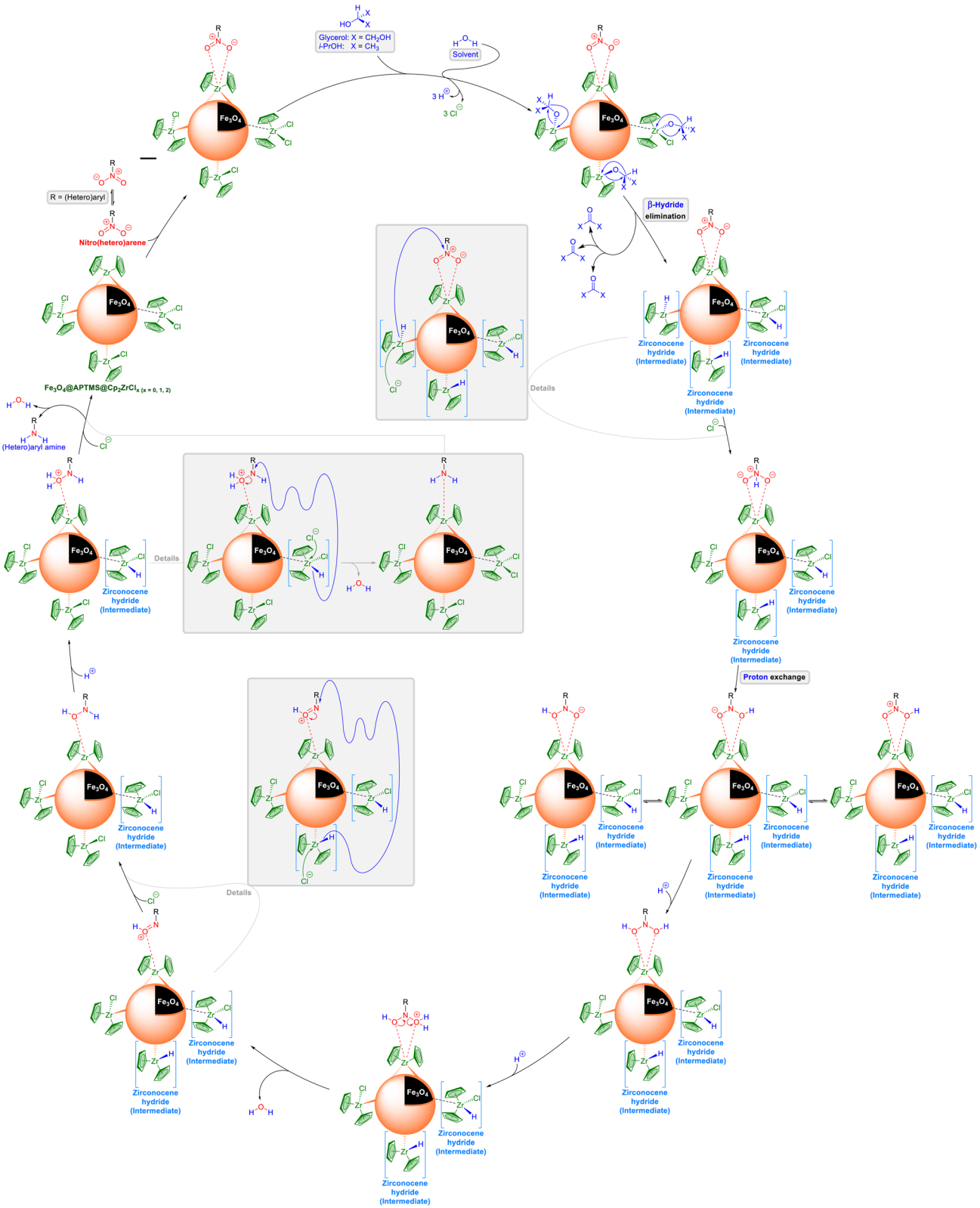

Scheme 2 Proposed mechanism for the reduction (hydrogenation) of nitro(hetero)arenes to the corresponding (hetero)aryl amines using glycerol or *i*-PrOH catalyzed by the Fe_3O_4@APTMS@Cp_2ZrCl_x ($x = 0, 1, 2$) nanocomposite through the hydridic route.

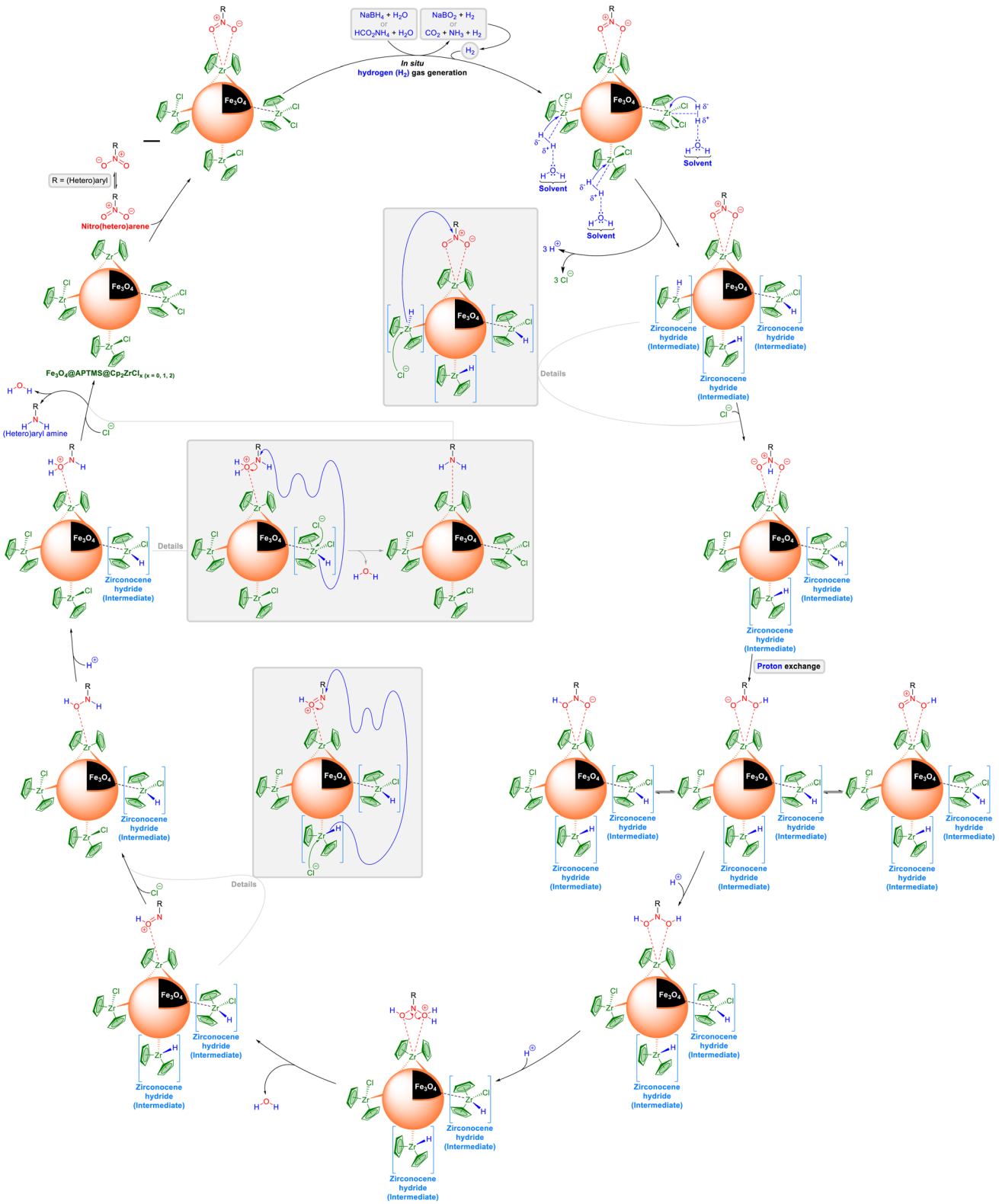

Scheme 3 Proposed mechanism for the reduction (hydrogenation) of nitro(hetero)arenes to the corresponding (hetero)aryl amines using $NaBH_4$ or HCO_2NH_4 catalyzed by the Fe_3O_4@APTMS@Cp_2ZrCl_x ($x = 0, 1, 2$) nanocomposite.

Table 2 Green and convenient one-pot two-step reductive acetylation of nitro(hetero)arenes to the corresponding *N*-(hetero)aryl acetamides catalyzed by the Fe_3O_4@APTMS@Cp_2ZrCl_x (x = 0, 1, 2) nanocomposite[a]

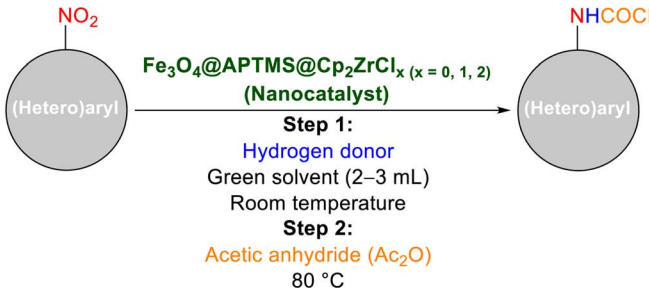

Strategy

Strategy V: **Nanocatalyst (7 mg)**; glycerol (2 mmol); H_2O; Ac_2O (1 mmol); 65–118 min; 80–96% (Current work).
Strategy VI: **Nanocatalyst (7 mg)**; *i*-PrOH (2 mmol); H_2O; Ac_2O (1 mmol); 85–150 min; 70–96% (Current work).
Strategy VII: **Nanocatalyst (5 mg)**; $NaBH_4$ (2 mmol); H_2O; Ac_2O (1 mmol); 15–60 min; 75–95% (Current work).
Strategy VIII: **Nanocatalyst (5 mg)**; HCO_2NH_4 (2 mmol); H_2O : PEG-400 (1 : 1); Ac_2O (1 mmol); 75–145 min; 77–96% (Current work).

			Strategy			
Entry	Substrate	Product	Strategy V	Strategy VI	Strategy VII	Strategy VIII
1	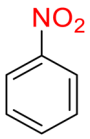	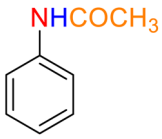	Time = 75 min Yield = 96% TON = 336.84 TOF = 4.49	Time = 85 min Yield = 96% TON = 336.84 TOF = 3.96	Time = 15 min Yield = 95% TON = 467.98 TOF = 31.20	Time = 75 min Yield = 96% TON = 472.90 TOF = 6.30
2	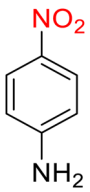	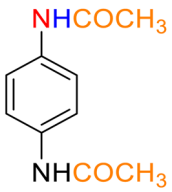	Time = 87 min Yield = 93% TON = 326.31 TOF = 3.75	Time = 120 min Yield = 81% TON = 284.21 TOF = 2.37	Time = 25 min Yield = 91% TON = 448.27 TOF = 17.93	Time = 100 min Yield = 89% TON = 438.42 TOF = 4.38
3	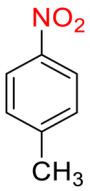	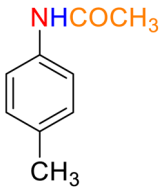	Time = 67 min Yield = 92% TON = 322.81 TOF = 4.82	Time = 95 min Yield = 88% TON = 308.77 TOF = 3.25	Time = 20 min Yield = 92% TON = 453.20 TOF = 22.66	Time = 85 min Yield = 91% TON = 448.27 TOF = 5.27
4	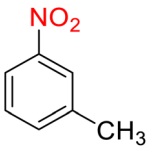	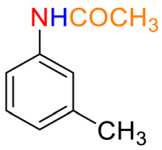	Time = 70 min Yield = 85% TON = 298.24 TOF = 4.26	Time = 125 min Yield = 86% TON = 301.75 TOF = 2.41	Time = 25 min Yield = 90% TON = 443.35 TOF = 17.71	Time = 88 min Yield = 85% TON = 418.72 TOF = 4.76
5		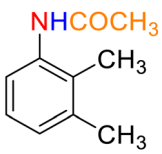	Time = 118 min Yield = 86% TON = 301.75 TOF = 2.56	Time = 150 min Yield = 80% TON = 280.70 TOF = 1.87	Time = 27 min Yield = 86% TON = 423.64 TOF = 15.69	Time = 120 min Yield = 83% TON = 408.87 TOF = 3.41
6	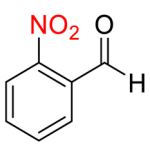	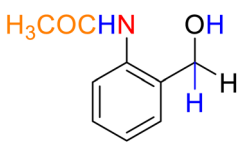	Time = 115 min Yield = 80% TON = 280.70 TOF = 2.44	Time = 150 min Yield = 70% TON = 245.61 TOF = 1.64	Time = 55 min Yield = 75% TON = 369.46 TOF = 6.72	Time = 145 min Yield = 77% TON = 379.31 TOF = 2.61

Table 2 (*Contd.*)

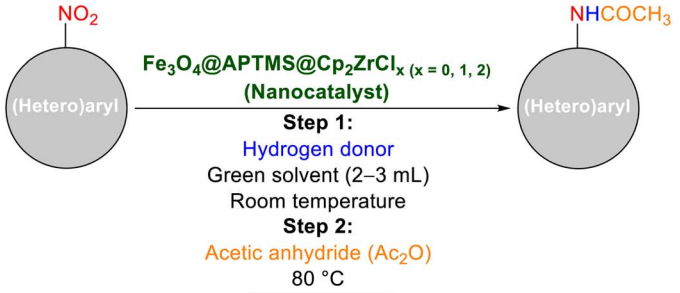

Strategy

Strategy V: Nanocatalyst (7 mg); glycerol (2 mmol); H_2O; Ac_2O (1 mmol); 65–118 min; 80–96% (Current work).
Strategy VI: Nanocatalyst (7 mg); *i*-PrOH (2 mmol); H_2O; Ac_2O (1 mmol); 85–150 min; 70–96% (Current work).
Strategy VII: Nanocatalyst (5 mg); $NaBH_4$ (2 mmol); H_2O; Ac_2O (1 mmol); 15–60 min; 75–95% (Current work).
Strategy VIII: Nanocatalyst (5 mg); HCO_2NH_4 (2 mmol); H_2O : PEG-400 (1 : 1); Ac_2O (1 mmol); 75–145 min; 77–96% (Current work).

			Strategy			
Entry	Substrate	Product	Strategy V	Strategy VI	Strategy VII	Strategy VIII
7	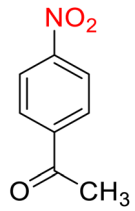	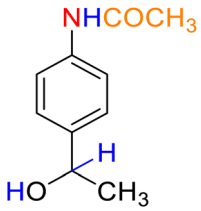	Time = 65 min Yield = 88% TON = 308.77 TOF = 4.75	Time = 115 min Yield = 85% TON = 298.24 TOF = 2.59	Time = 35 min Yield = 85% TON = 418.71 TOF = 11.96	Time = 110 min Yield = 88% TON = 433.50 TOF = 3.94
8	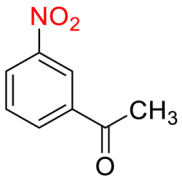	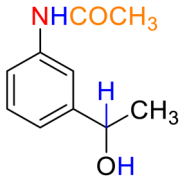	Time = 70 min Yield = 86% TON = 301.75 TOF = 4.31	Time = 120 min Yield = 81% TON = 284.21 TOF = 2.37	Time = 40 min Yield = 80% TON = 394.09 TOF = 9.85	Time = 115 min Yield = 82% TON = 403.94 TOF = 3.51
9	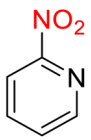	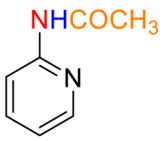	Time = 90 min Yield = 84% TON = 294.74 TOF = 3.27	Time = 150 min Yield = 85% TON = 298.24 TOF = 1.99	Time = 60 min Yield = 81% TON = 399.01 TOF = 6.65	Time = 140 min Yield = 88% TON = 433.50 TOF = 3.10

[a] (a) TON (turnover number) = [(mol of product formed)/(mol of catalyst used)]. (b) TOF (turnover frequency) = [(mol of product formed)/(mol of catalyst used) × (time)]. (c) The TON and TOF values were calculated based on the existing amount of zirconium (Zr) in the structure of the as-prepared Fe_3O_4@APTMS@Cp_2ZrCl_x $(x = 0, 1, 2)$ nanocomposite based on ICP-OES analysis. (d) In entry 2, the amount of acetic anhydride (Ac_2O) used was 2 mmol.

diagram (Fig. 4, section d) of the mentioned nanocomposite confirmed the presence of the carbon (C), nitrogen (N), oxygen (O), silicon (Si), chlorine (Cl), ferrite (Fe), and zirconium (Zr) elements. Furthermore, the inductively coupled plasma-optical emission spectrometry (ICP-OES) analysis (Fig. 4, section e) demonstrated the exact amounts of Fe (52.75 w%) and Zr (3.72 w%) in the as-prepared core–shell-type Fe_3O_4@APTMS@Cp_2ZrCl_x $(x = 0, 1, 2)$ nanocomposite structure.

The analysis using an alternating gradient force magnetometer (AGFM) showed that the as-synthesized Fe_3O_4@APTMS@Cp_2ZrCl_x $(x = 0, 1, 2)$ nanocomposite exhibits superparamagnetic behavior and sufficient saturation magnetization (M_s) for effective magnetic recycling performance (Fig. 4, section f). On the other hand, the thermogravimetric analysis (TGA) shows that the zirconocene-containing catalytic system exhibits excellent thermal stability for the organic transformations carried out at temperatures ranging from room temperature to 80 °C (Fig. 4, section g). The TGA diagram (Fig. 4, section g) indicates that the structure of this nanocomposite remains completely stable up to 80 °C, with only a 0.19% weight

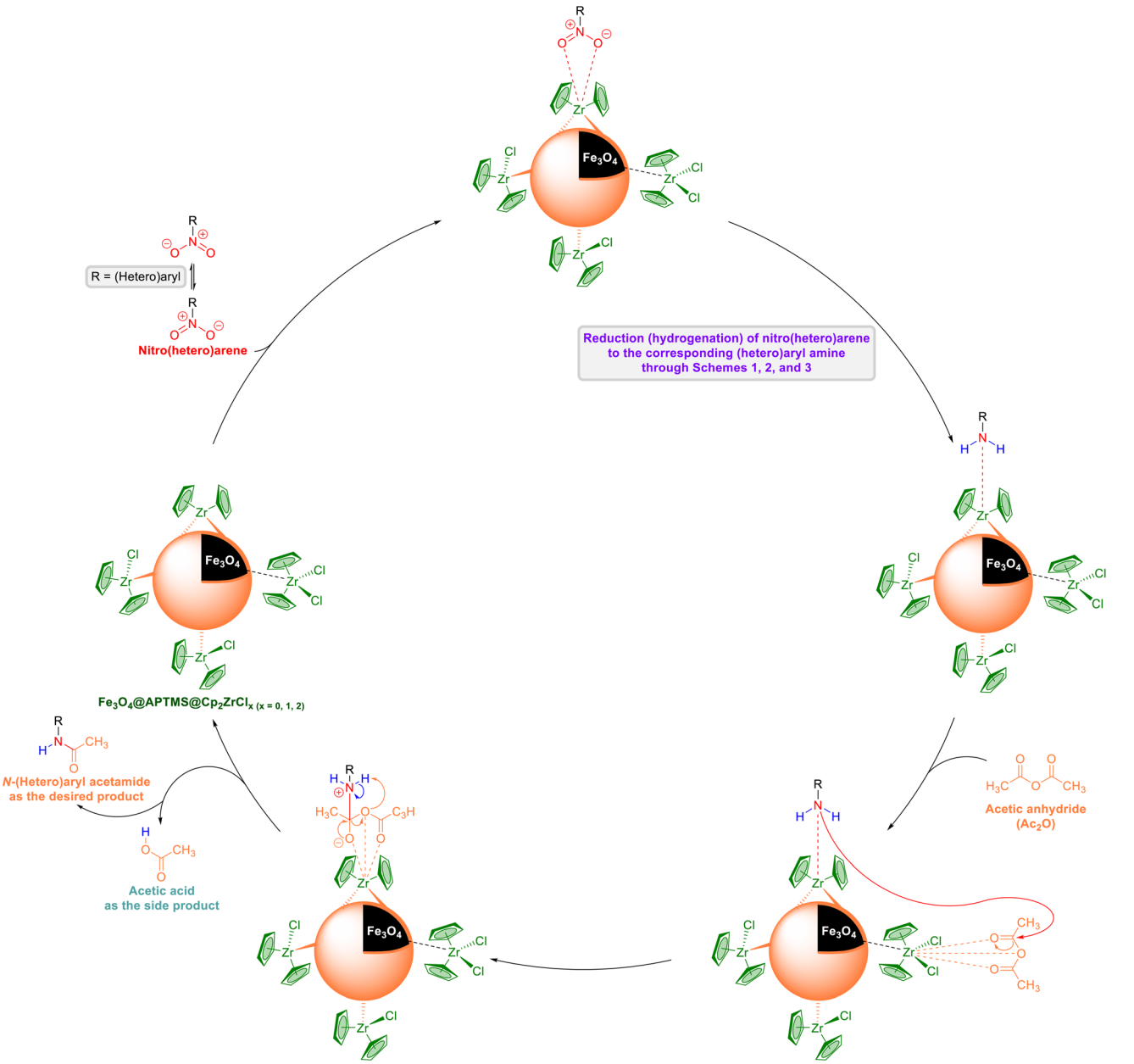

Scheme 4 Plausible mechanism for the convenient one-pot two-step reductive acetylation of nitro(hetero)arenes to the corresponding *N*-(hetero)aryl acetamides catalyzed by the Fe_3O_4@APTMS@Cp_2ZrCl_x $(x = 0, 1, 2)$ nanocomposite.

loss observed at this temperature. Interestingly, the superparamagnetic zirconium-containing nanocomposite experiences a 21% weight loss at 800 °C.

The nitrogen (N_2) gas adsorption–desorption analysis (Fig. 4, section h) of the as-synthesized Fe_3O_4@APTMS@Cp_2ZrCl_x $(x = 0, 1, 2)$ nanocomposite reveals an isotherm shape approximately classified as type IV with a H_1-type hysteresis loop. Also, the mentioned analysis demonstrated that the specific surface area (S_{BET}) and total pore volume (V_{total}) values of the as-prepared mesoporous Zr-containing nanocomposite were 81.31 m^2 g^{-1} and 0.26 cm^3 g^{-1}, respectively (Fig. 4, section h).

2.2. Reduction (hydrogenation) of nitro(hetero)arenes to the corresponding (hetero)aryl amines

It should be noted that Zeynizadeh and Sepehraddin reported the first catalytic application of the as-prepared Fe_3O_4@APTMS@Cp_2ZrCl_x $(x = 0, 1, 2)$ nanocomposite for the reduction (hydrogenation) of nitro-containing (hetero)aromatic compounds to the corresponding amines using glycerol as a reducing (hydrogen donor) agent in water at room temperature (Fig. 2 and Table 1).[14] In the current work, we tried to investigate the effect of other easily accessible reducing (hydrogen donors) agents, namely isopropanol (*i*-PrOH), sodium borohydride ($NaBH_4$), and ammonium formate

Table 3 Comparison of the catalytic activity of the as-prepared Fe_3O_4@APTMS@$Cp_2ZrCl_{x\ (x\ =\ 0,\ 1,\ 2)}$ nanocomposite with those of the literature samples reported upon reduction (hydrogenation) and one-pot reductive acetylation of nitrobenzene[a]

Part A

Entry	Reaction conditions	Time	Yield	Ref.
A1	Fe_3O_4@APTMS@$Cp_2ZrCl_{x\ (x\ =\ 0,\ 1,\ 2)}$ (7 mg); glycerol (2 mmol); H_2O; r. t.	40 min	96%	14
A2	Fe_3O_4@APTMS@$Cp_2ZrCl_{x\ (x\ =\ 0,\ 1,\ 2)}$ (7 mg); *i*-PrOH (2 mmol); H_2O; r. t.	60 min	97%	[a]
A3	Fe_3O_4@APTMS@$Cp_2ZrCl_{x\ (x\ =\ 0,\ 1,\ 2)}$ (5 mg); $NaBH_4$ (2 mmol); H_2O; r. t.	10 min	95%	[a]
A4	Fe_3O_4@APTMS@$Cp_2ZrCl_{x\ (x\ =\ 0,\ 1,\ 2)}$ (5 mg); HCO_2NH_4 (2 mmol); H_2O : PEG-400 (1 : 1); r. t.	60 min	97%	[a]
A5	Fe_3O_4/*f*-MWCNT-CS-Glu/Ni^{II} (5 mg); $NaBH_4$ (2 mmol); H_2O; 60 °C	4 min	98%	13*a*
A6	Fe_3O_4@SiO_2@KCC-1@MPTMS@Cu^{II} (10 mg); $NaBH_4$ (2 mmol); H_2O; 60 °C	5 min	98%	13*d*
A7	(7 wt%) Pd/C (30 mg); $NaBH_4$ (2 mmol); H_2O; reflux	7 min	93%	13*f*
A8	$CuFe_2O_4$ (48 mg); $NaBH_4$ (2 mmol); H_2O; reflux	50 min	95%	13*i*
A9	$Fe_2Se_2CO_9$ (3 mol%); $NH_2NH_2{\cdot}H_2O$ (2 mmol); H_2O; 110 °C	15 min	89%	20
A10	$Ni(OH)_2$@PANI-1 (3.2 mol%); $NaBH_4$ (10 mmol); H_2O; reflux	1.5 h	85%	21
A11	Cu-BTC@Fe_3O_4 (15 mg); $NaBH_4$ (4 mmol); CH_3CH_2OH : H_2O (3 : 1); 45 °C	3 h	99%	22
A12	IT-MHAP-Ag (60 mg); $NaBH_4$ (5 mmol); H_2O; reflux	25 min	98%	23
A13	PSeCN/Ag (20 mg); $NaBH_4$ (5 mmol); H_2O; 75 °C	25 min	99%	24
A14	CoOCN (20 mg); $NH_2NH_2{\cdot}H_2O$ (2 mmol); H_2O; 100 °C	5 h	84%	25
A15	Fe_3O_4@SiO_2@KIT-6@2-ATP@Cu^{I} (20 mg); $NaBH_4$ (5 mmol); H_2O; r. t.	60 min	89%	26
A16	$[C_4(DABCO)_2]{\cdot}NiCl_4$ (80 mg); $NaBH_4$ (3.5 mmol); H_2O; 70 °C	1 min	98%	27
A17	Ru-*N*,*P*-C_{BM} (0.02 mol% of Ru); $NaBH_4$ (5 mmol); CH_3CH_2OH : H_2O (1 : 1); r. t.	60 min	98%	28
A18	MBC-PVIm/Pd (30 mg); $NaBH_4$ (3 mmol); H_2O; 50 °C	30 min	99%	29
A19	SiO_2/Fe_3O_4-SiO_2-NH_2/Cu-Ag (5 mg); $NaBH_4$ (2 mmol); H_2O; 70 °C	5 min	83%	30
A20	rGO@Fe_3O_4/$ZrCp_2Cl_{x\ (x\ =\ 0,\ 1,\ 2)}$ (20 mg); $NH_2NH_2{\cdot}H_2O$ (2 mmol); CH_3CH_2OH; reflux	10 min	98%	31
A21	Se^0 (20 mol%); $NaBH_4$ (4 mmol); NaOH (1 mmol); H_2O; 100 °C	3 h	88%	32
A22	Fe_3O_4/GO–IL–Pd (50 mg); $NaBH_4$ (2 mmol); H_2O; 60 °C	10 min	95%	33
A23	Fe_3O_4/Biochar–Pd (10 mg); $NaBH_4$ (5 mmol); CH_3CH_2OH : H_2O (3 : 1); 70 °C	20 min	96%	34
A24	Cu-NPs (5 mol%); $NaBH_4$ (4 mmol); CH_3CH_2OH : H_2O (1 : 3); r. t.	2 h	99%	35

Part B

Entry	Reaction conditions	Time	Yield	Ref.
B1	Fe_3O_4@APTMS@$Cp_2ZrCl_{x\ (x\ =\ 0,\ 1,\ 2)}$ (7 mg); glycerol (2 mmol); H_2O; r. t.; Ac_2O (1 mmol); 80 °C	75 min	96%	[a]
B2	Fe_3O_4@APTMS@$Cp_2ZrCl_{x\ (x\ =\ 0,\ 1,\ 2)}$ (7 mg); *i*-PrOH (2 mmol); H_2O; r. t.; Ac_2O (1 mmol); 80 °C	85 min	96%	[a]
B3	Fe_3O_4@APTMS@$Cp_2ZrCl_{x\ (x\ =\ 0,\ 1,\ 2)}$ (5 mg); $NaBH_4$ (2 mmol); H_2O; r. t.; Ac_2O (1 mmol); 80 °C	15 min	95%	[a]
B4	Fe_3O_4@APTMS@$Cp_2ZrCl_{x\ (x\ =\ 0,\ 1,\ 2)}$ (5 mg); HCO_2NH_4 (2 mmol); H_2O : PEG-400 (1 : 1); r. t.; Ac_2O (1 mmol); 80 °C	75 min	96%	[a]
B5	Fe_3O_4/*f*-MWCNT-CS-Glu/Ni^{II} (5 mg); $NaBH_4$ (2 mmol); Ac_2O (1 mmol); H_2O; r. t.	5 min	97%	13*a*
B6	Fe_3O_4@SiO_2@KCC-1@MPTMS@Cu^{II} (10 mg); $NaBH_4$ (2 mmol); Ac_2O (1 mmol); H_2O; 60 °C	7 min	95%	13*d*
B7	(7 wt%) Pd/C (30 mg); $NaBH_4$ (2 mmol); Ac_2O (1 mmol); H_2O; reflux	8 min	88%	13*f*
B8	$Cu(Hdmg)_2$ (10 mol%); $NaBH_4$ (3 mmol); EtOAc; 60 °C	170 min	97%	13*h*
B9	$[C_4(DABCO)_2]{\cdot}NiCl_4$ (80 mg); $NaBH_4$ (3.5 mmol); H_2O; Ac_2O (1 mmol); 70 °C	2 min	98%	27
B10	rGO@Fe_3O_4/$ZrCp_2Cl_{x\ (x\ =\ 0,\ 1,\ 2)}$ (20 mg); $NH_2NH_2{\cdot}H_2O$ (2 mmol); Ac_2O (2 mmol); CH_3CH_2OH; reflux	15 min	97%	31
B11	(2 wt%) Pd/(5 wt%) Sn–Al_2O_3 (50 mg); H_2 atmosphere; Ac_2O (1 mmol); H_2O; r. t.	3 h	98%	36
B12	f-ZCu (100 mg); $NH_2NH_2{\cdot}H_2O$ (2 mmol); CH_3CO_2H; 110 °C	6 h	82%	37

[a] Present work.

(HCO_2NH_4), on the stated organic transformation in the presence of the mentioned superparamagnetic core–shell-type zirconocene-containing nanocatalyst. For this purpose, we carried out several tests to find the optimal reaction conditions (Table S1†). After this stage, we investigated the scope and limitations of the new and green reduction (hydrogenation) protocols using various types of nitro(hetero) arenes (Table 1). As shown in Table 1, the experimental results indicate that substrates with electron-donating and electro-withdrawing groups are also well tolerated under optimized reaction conditions. Besides, the turnover numbers (TONs) and turnover frequencies (TOFs) of the

Table 4 Recoverability and reusability experiments of the as-prepared Fe_3O_4@APTMS@$Cp_2ZrCl_{x\ (x\ =\ 0,\ 1,\ 2)}$ nanocomposite

	Reaction strategy															
	I		II		III		IV		V		VI		VII		VIII	
Run number	Time (min)	Yield (%)	Time (min)	Yield (%)	Time (min)	Yield (%)	Time (min)	Yield (%)	Time (min)	Yield (%)	Time (min)	Yield (%)	Time (min)	Yield (%)	Time (min)	Yield (%)
1	40	96	60	97	10	95	60	97	75	96	85	96	15	95	75	96
2	40	95	60	97	10	95	60	97	75	95	85	96	15	95	75	96
3	45	94	65	96	12	94	65	96	80	94	90	94	20	94	80	94
4	45	94	65	96	12	94	65	95	80	92	90	91	20	92	80	91
5	50	93	70	95	14	93	70	94	85	90	95	90	25	91	90	90

Fe_3O_4@APTMS@$Cp_2ZrCl_{x\ (x\ =\ 0,\ 1,\ 2)}$ nanocatalyst in these reactions were calculated and are listed in Table 1. Importantly, as indicated in Table 1, the values of TONs and TOFs were satisfactory and acceptable. It is important to note that the exact mechanism for the reduction (hydrogenation) of nitro(hetero)arenes to the corresponding (hetero)aryl amines using introduced hydrogen donors in the presence of the as-prepared Fe_3O_4@APTMS@$Cp_2ZrCl_{x\ (x\ =\ 0,\ 1,\ 2)}$ nanocomposite as the heterogeneous mesoporous nanocatalyst is unclear. Despite this issue, we introduced different plausible mechanisms (two mechanisms to illustrate the role and behavior of glycerol or *i*-PrOH (Schemes 1 and 2) and also one reaction mechanism (Scheme 3) for $NaBH_4$ or HCO_2NH_4) in the presence of the mentioned zirconocene-containing nanocatalyst based on our observations and literature data.[15,17]

As illustrated in Schemes 1 and 2, when the nitro(hetero) arene reduction (hydrogenation) reaction was carried out with glycerol or *i*-PrOH as the reducing (hydrogen donor) agent in the presence of the as-prepared Fe_3O_4@APTMS@$Cp_2ZrCl_{x\ (x\ =\ 0,\ 1,\ 2)}$ nanocatalyst in water, we suspect that this reaction may have occurred *via* two different pathways, including direct hydrogen transfer and the hydridic route, based on literature data. In the first pathway (Scheme 1), *viz.* direct hydrogen transfer, glycerol or *i*-PrOH is activated by attaching to the zirconium metal. Subsequently, by performing a Meerwein–Ponndorf–Verley (MPV)-like reaction, hydrogen is transferred directly to the nitro(hetero)arene molecule. Conversely, in the second pathway (Scheme 2), *viz.* hydridic route, after the activation of glycerol or *i*-PrOH by attaching to the zirconium metal, the β-hydride elimination causes the formation of a zirconocene hydride intermediate, which is capable of the reduction (hydrogenation) of nitro(hetero)arene to the corresponding (hetero)aryl amine through the transfer hydrogenation process. On the other hand and as shown in Scheme 3, when the reduction (hydrogenation) reaction was conducted with $NaBH_4$ or HCO_2NH_4 as the reducing (hydrogen donor) agent in the presence of the as-prepared Fe_3O_4@APTMS@$Cp_2ZrCl_{x\ (x\ =\ 0,\ 1,\ 2)}$ nanocatalyst in the water solvent (or the H_2O:PEG-400 mixture solvent), we observed the production of hydrogen (H_2) gas inside the reaction vessel. Based on this observation, we believe that the *in situ*-generated H_2 gas diffused in the reaction environment and was then activated by the zirconium (Zr) metal and the electron pairs of oxygen belonging to the water molecule. After that, replacing zirconium-attached chlorine with partially negative charge hydrogen caused the formation of the zirconocene hydride intermediate, which was one of the fundamental intermediates in the mentioned reduction (hydrogenation) reaction. Subsequently, the step-by-step hydrogen transfer process from the zirconocene hydride intermediate to the nitro(hetero)arene molecule, which was followed by the proton exchange and then the elimination of two water molecules, led to the reduction (hydrogenation) of the nitro(hetero)arene molecule to the corresponding (hetero)aryl amine.

2.3. One-pot two-step reductive acetylation of nitro(hetero) arenes to the corresponding *N*-(hetero)aryl acetamides

Developing effective and straightforward synthetic strategies for constructing amides, which are prevalent functional and structural elements in drugs, agrochemicals, peptides, proteins, and many others, is highly valuable in organic synthesis.[18] From the green chemistry point of view, one-pot reactions are always the best choice for chemists due to their simplicity, time- and cost-effectiveness, and many others.[19] In this regard, and following successful reduction (hydrogenation) strategies for nitro(hetero)arenes, we decided to introduce new one-pot two-step reductive acetylation approaches for the efficient and green synthesis of *N*-(hetero)aryl acetamides from nitro(hetero) arenes. For this purpose, in the second step of the mentioned one-pot organic transformation (*viz.* acetylation), we used acetic anhydride (Ac_2O) as an acetylating agent under different reaction temperature conditions (80 °C) rather than step one (room temperature). Under these reaction conditions, we successfully prepared diverse *N*-(hetero)aryl acetamide derivatives (Table 2). Notably, based on the amount of catalyst used, our protocols have acceptable reaction times, yields, TONs, and TOFs (Table 2). Furthermore, a plausible mechanism for the current one-pot two-step reductive acetylation reactions is depicted in Scheme 4. Briefly, after the reduction (hydrogenation) of the nitro(hetero)arene molecule to the corresponding (hetero)aryl amine, which is illustrated in Schemes 1–3, the *in situ* obtained (hetero)aryl amine compound was acetylated through attacking Ac_2O, which was activated by the as-prepared Fe_3O_4@APTMS@$Cp_2ZrCl_{x\ (x\ =\ 0,\ 1,\ 2)}$ nanocatalyst (Scheme 4).

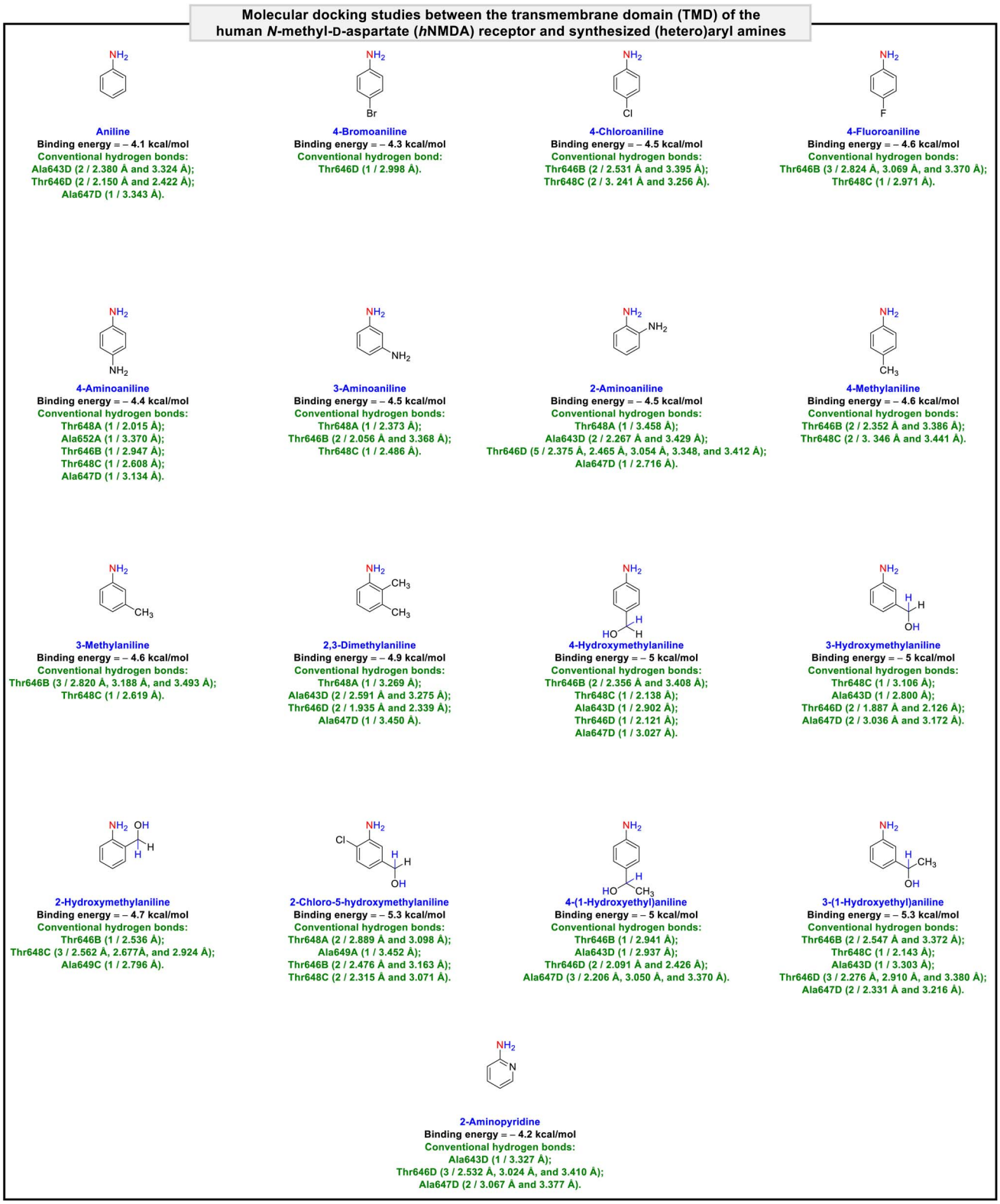

Fig. 5 Molecular docking studies between the transmembrane domain (TMD) of the human *N*-methyl-D-aspartate (*h*NMDA) receptor and synthesized (hetero)aryl amines.

2.4. A comparative study

The practicality of the current diverse green procedures for the convenient reduction (hydrogenation) and one-pot two-step reductive acetylation of nitro(hetero)arenes in the presence of the superparamagnetic core–shell-type Fe_3O_4@APTMS@Cp_2ZrCl_x (x = 0, 1, 2) nanocomposite as a powerful

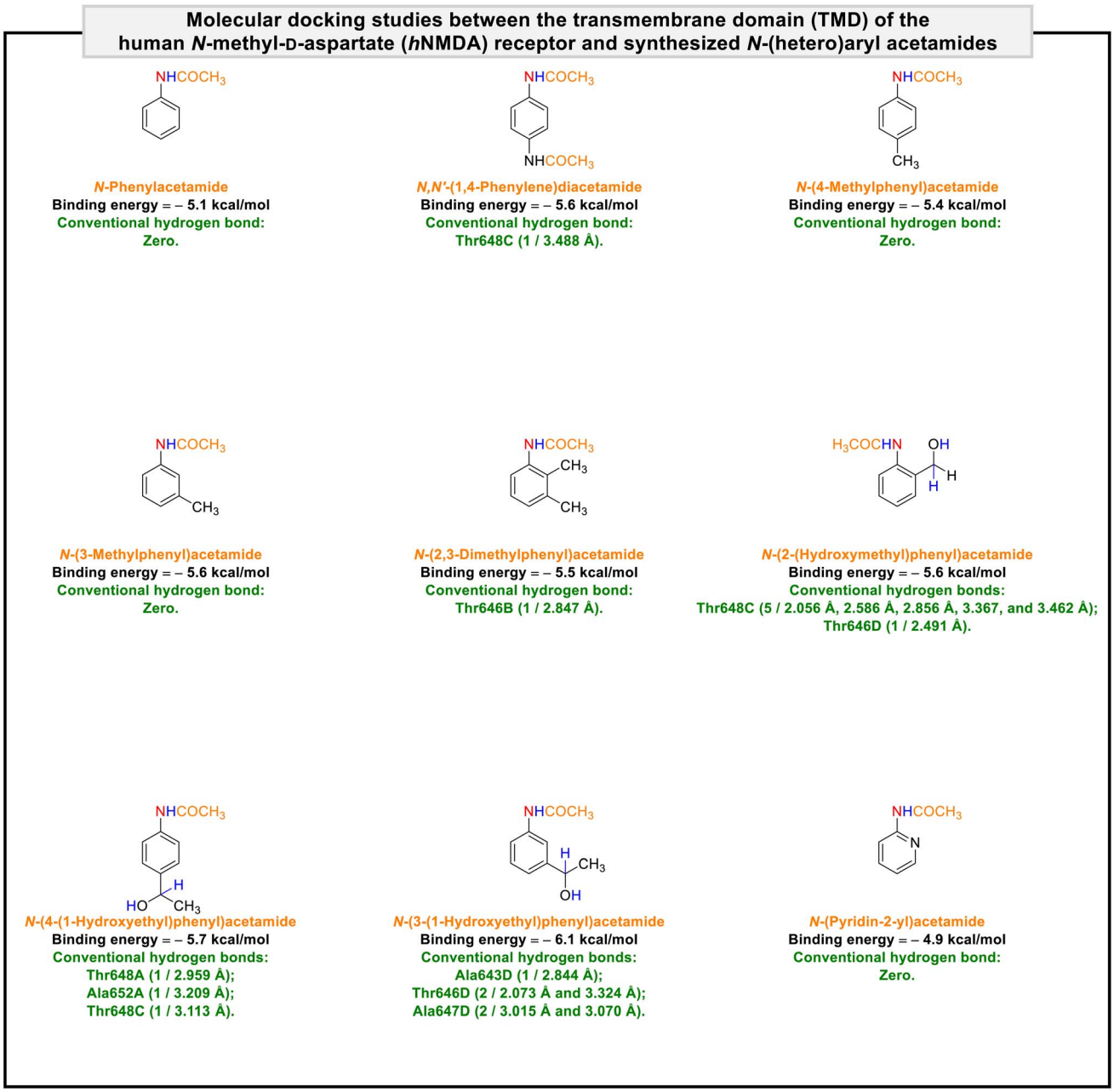

Fig. 6 Molecular docking studies between the transmembrane domain (TMD) of the human *N*-methyl-D-aspartate (*h*NMDA) receptor and synthesized *N*-(hetero)aryl acetamides.

catalytic system is highlighted by a comparison of the obtained results with those of some of the previously reported methods on the mentioned organic transformations (Table 3). The stated comparative study demonstrated that the current green synthetic strategies have a relatively suitable place in terms of efficiency compared to the previous protocols.

2.5. Recoverability and reusability experiments

In the next phase of this work, we assessed the recyclability and reusability of the as-prepared core–shell-type Fe_3O_4@-APTMS@Cp_2ZrCl_x $(x = 0, 1, 2)$ nanocomposite. As shown in Table 4, we conducted the desired reaction strategies over five consecutive runs without observing a significant loss in the catalytic activity of the zirconocene-containing nanocatalytic system.

2.6. Molecular docking and ADMET studies

It is worth noting that NMDA receptors have a hetero-tetrameric structure consisting of an amino-terminal domain (ATD), a ligand-binding domain (LBD), and a transmembrane domain (TMD). To explore the protein–ligand interactions between the transmembrane domain (TMD) of the human *N*-

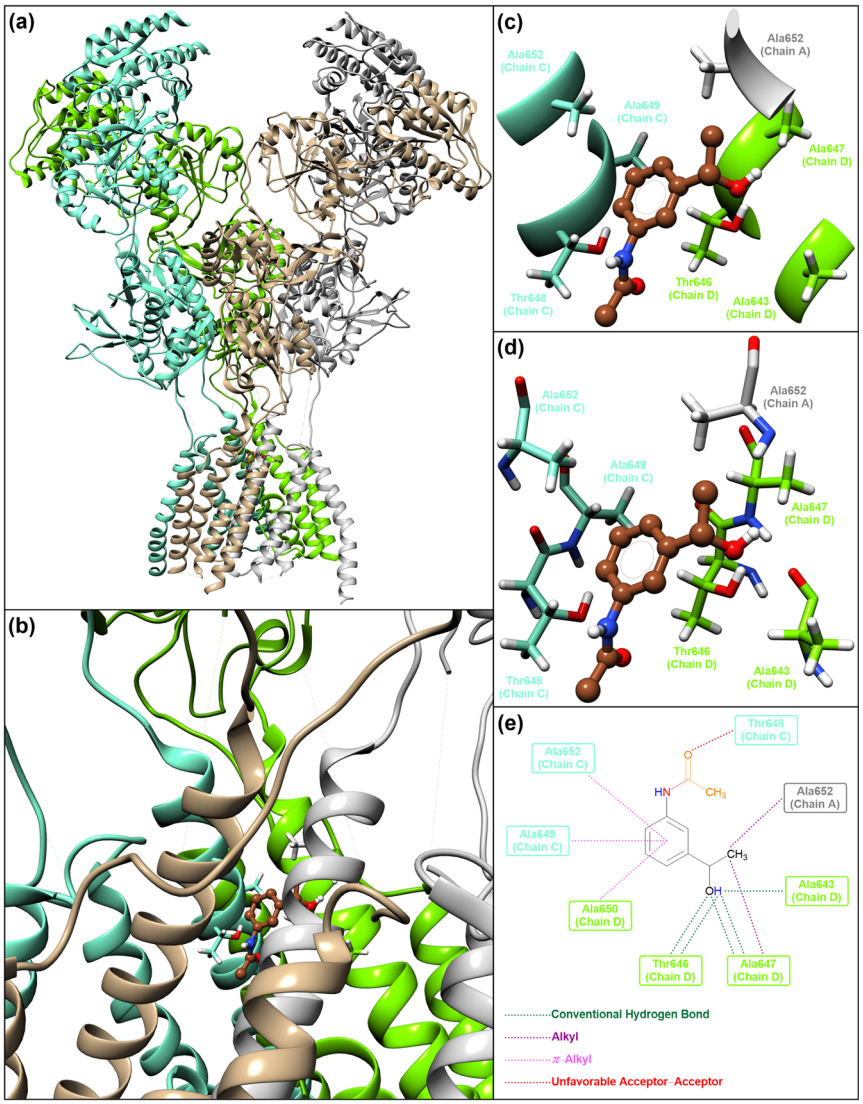

Fig. 7 Close-up views (3D and 2D) of *N*-(3-(1-hydroxyethyl)phenyl)acetamide in the TMD of the *h*NMDA receptor.

methyl-D-aspartate (*h*NMDA) receptor (PDB ID: 7EU7) and our obtained compounds (*viz.* (hetero)aryl amines and *N*-(hetero) aryl acetamides), we carried out a molecular docking process using AutoDock Vina as an open-source program for doing molecular docking along with UCSF Chimera as a graphical user interface. The obtained binding energies of the molecular docking investigations ranged from −4.1 kcal mol^{-1} to −5.3 kcal mol^{-1} for (hetero)aryl amines (Fig. 5) and −4.9 kcal mol^{-1} to −6.1 kcal mol^{-1} for *N*-(hetero)aryl acetamides (Fig. 6). From the binding energy point of view, the accomplished results verified that *N*-(3-(1-hydroxyethyl) phenyl)acetamide with a binding energy of −6.1 kcal mol^{-1} is slightly better than other compounds. As shown in Fig. 7, *N*-(3-(1-hydroxyethyl)phenyl)acetamide was able to form five conventional hydrogen bonds with Ala643D (2.844 Å), Thr646D (2.073 Å and 3.324 Å), and Ala647D (3.015 Å and 3.070 Å) of the *h*NMDA receptor TMD. The mentioned compound also has interactions with residues Ala652A (alkyl), Thr648C (unfavorable acceptor–acceptor), Ala649C (π–alkyl), Ala652C (π–alkyl), Ala647D (alkyl), and Ala650D (π–alkyl) (Fig. 7). It is worthwhile to note that we conducted comparative molecular docking studies between *N*-(3-(1-hydroxyethyl) phenyl)acetamide as our hit compound and related medicinal compounds (including Amantadine, Dextromethorphan, Dextrorphan, Dizocilpine, Esketamine, and Huperzine A), and *N*-(3-(1-hydroxyethyl)phenyl)acetamide appears to have a distinct advantage for this purpose, from the binding energy point of view (Fig. 8). Understanding the absorption, distribution, metabolism, excretion, and toxicity (ADMET) parameters is essential for developing new drugs and drug-like molecules.[38] In this context, we utilized the free web tool SwissADME, provided by the Swiss Institute of Bioinformatics (**http://www.swissadme.ch**),[39] to assess the ADME properties of *N*-(3-(1-hydroxyethyl)phenyl)acetamide. The *in silico* data related to physicochemical properties and lipophilicity, water solubility, pharmacokinetics, and drug-likeness and

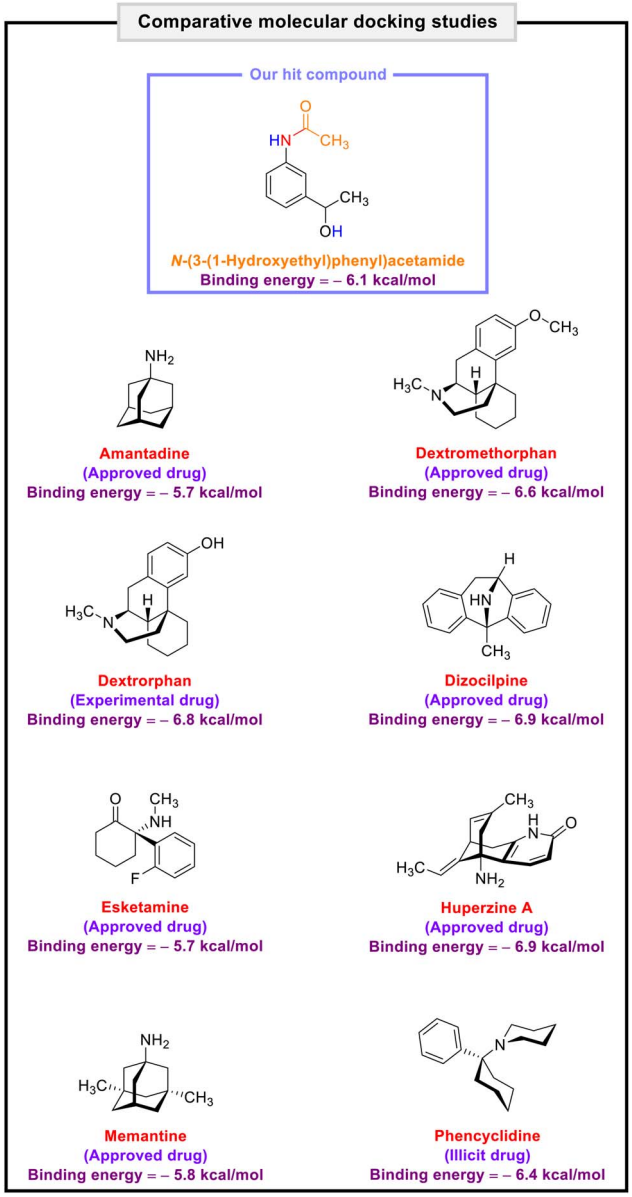

Fig. 8 Comparative molecular docking studies.

medicinal chemistry of the obtained *N*-(3-(1-hydroxyethyl) phenyl)acetamide compound have been collected and are shown in Fig. 9. Interestingly, the attained results demonstrated that *N*-(3-(1-hydroxyethyl)phenyl)acetamide generally possesses drug-like behavior because it could successfully pass the four of five fundamental drug-likeness filters, including Lipinski (Pfizer), Ghose (Amgen), Veber (GSK), and Egan (Pharmacia). Furthermore, the mentioned organic compound gratifyingly passed pan assay interference structures (PAINS) and Brenk filters. Also, the bioavailability radar of the synthesized *N*-(3-(1-hydroxyethyl)phenyl)acetamide is depicted in Fig. 9. On the other hand, the BOILED-Egg plot of *N*-(3-(1-hydroxyethyl)phenyl)acetamide shows high gastrointestinal (GI) absorption and has blood–brain barrier (BBB) permeability, and the red dot as a P-glycoprotein non-substrate (PGP–) demonstrates predictions that the mentioned organic molecule cannot be effluxed from the central nervous system (CNS) by PGP (Fig. 9). Besides, the *in silico* toxicity evaluation was carried out using an online server, Deep-PK (**https://biosig.lab.uq.edu.au/deeppk/**).[40] As shown in Fig. 9, the results of the *in silico* Ames mutagenesis, avian, and bee toxicity tests were safe for the mentioned synthesized compound.

3. Experimental

3.1. Reagents, samples, and apparatus

All starting materials, reagents, and solvents were commercially available (purchased from Merck, Sigma-Aldrich, and Fluka companies) and used directly without further purification. The FT-IR spectra were recorded using a Thermo Nicolet Nexus 670 spectrometer. The ^{1}H and $^{13}C\{H\}$ NMR spectra were recorded on a Bruker Avance 300 MHz spectrometer at 300 MHz and 75 MHz, respectively. The crystalline structure of the as-prepared zirconocene-containing nanocomposite was investigated by PXRD on a Philips PANalytical X'Pert Pro diffractometer (Netherlands). The SEM image and EDX diagram of the as-prepared Fe_3O_4@APTMS@Cp_2ZrCl_x $(x = 0, 1, 2)$ nanocomposite were acquired using an FESEM-TESCAN MIRA3 electron microscope. The exact amounts of Fe and Zr were detected by inductively coupled plasma-optical emission spectrometry (ICP-OES). The magnetic properties of the mentioned zirconocene-containing nanocomposite were analyzed on an alternating gradient force magnetometer (AGFM) at room temperature. The thermogravimetric analysis (TGA) was performed with a Shimadzu DTG-60 instrument under a nitrogen atmosphere. The nitrogen (N_2) gas adsorption–desorption isotherms were measured using a Belsorp-Max (BEL Japan, Inc). Thin-layer chromatography (TLC) was used to determine the purity of products and monitor the reaction over a silica gel 60 F_{254} aluminum sheet.

3.2. Preparation of the superparamagnetic core–shell-type Fe_3O_4@APTMS@Cp_2ZrCl_x $(x = 0, 1, 2)$ nanocomposite

The superparamagnetic core–shell-type Fe_3O_4@APTMS@Cp_2ZrCl_x $(x = 0, 1, 2)$ nanocomposite was prepared accurately through our previous research papers.[14–16]

3.3. General procedure for the green reduction (hydrogenation) of nitro(hetero)arenes to (hetero)aryl amines catalyzed by the as-prepared Fe_3O_4@APTMS@Cp_2ZrCl_x $(x = 0, 1, 2)$ nanocomposite

As a representative example, in a round-bottom flask (10 mL) equipped with a magnetic stirrer, a mixture of nitrobenzene (1 mmol) and H_2O (2–3 mL) was prepared. Then, 5 mg of the as-prepared superparamagnetic core–shell-type Fe_3O_4@APTMS@Cp_2ZrCl_x $(x = 0, 1, 2)$ nanocomposite was added, and the mixture was stirred. In the next step, $NaBH_4$ (2 mmol) was added, and the resulting mixture was continuously stirred at room temperature for ten minutes. After the completion of the reaction, the mentioned zirconocene-containing catalytic system was separated from the reaction pot using an external

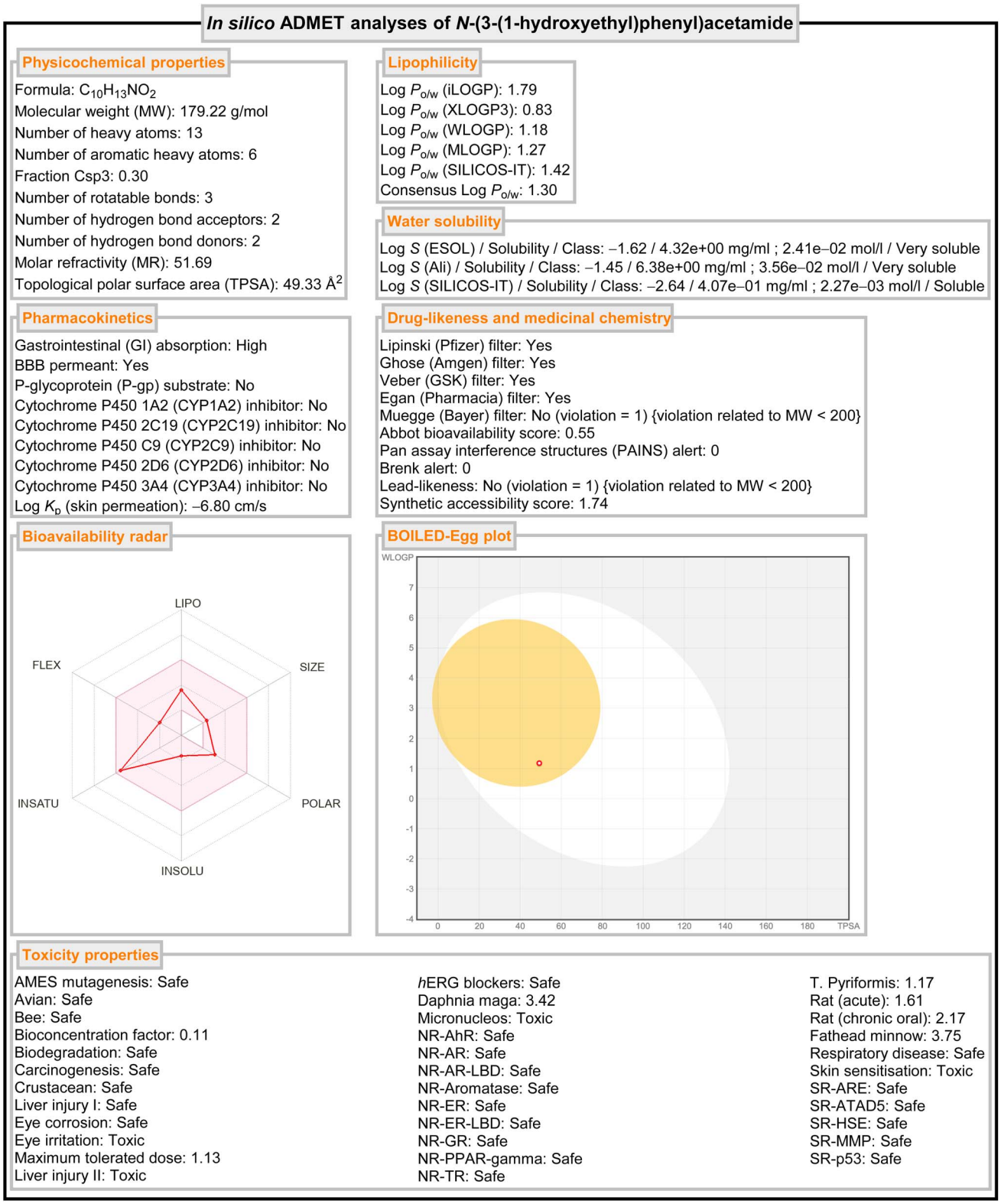

Fig. 9 ADMET analyses of *N*-(3-(1-hydroxyethyl)phenyl)acetamide.

magnet. The reaction mixture was extracted with ethyl acetate (EtOAc) (2 × 5 mL) and then dried over anhydrous sodium sulfate (Na_2SO_4). Lastly, the solvent was evaporated under reduced pressure followed by further purification using short-column chromatography over silica gel which afforded pure liquid aniline in 95% yield.

3.4. General procedure for the convenient one-pot two-step reductive acetylation of nitro(hetero)arenes to *N*-(hetero)aryl acetamides catalyzed by the as-prepared Fe_3O_4@APTMS@Cp_2ZrCl_x (x = 0, 1, 2) nanocomposite

As an example, in a round-bottom flask (10 mL) equipped with a magnetic stirrer, a mixture of nitrobenzene (1 mmol) and H_2O (2–3 mL) was prepared, and then, 5 mg of the as-prepared core–shell-type Fe_3O_4@APTMS@Cp_2ZrCl_x (x = 0, 1, 2) nanocomposite was added, and the mixture was stirred. In the next step, $NaBH_4$ (2 mmol) was added, and the resulting mixture was continuously stirred at room temperature for ten minutes. After completion of the reduction (hydrogenation) step, acetic anhydride (Ac_2O) (1 mmol) was added to the reaction mixture, followed by stirring for a further five minutes at 80 °C. After the completion of the acetylation reaction, the mentioned superparamagnetic zirconocene-containing catalytic system was separated from the reaction pot using an external magnet. The reaction mixture was extracted with ethyl acetate (EtOAc) (2 × 5 mL) and then dried over anhydrous sodium sulfate (Na_2SO_4). Lastly, the solvent was evaporated under reduced pressure followed by further purification using short-column chromatography over silica gel affording the pure acetanilide in 95% yield.

3.5. *In silico* molecular docking and ADMET

The molecular docking simulation was carried out using AutoDock Vina (version 1.1.2) as an open-source program incorporating UCSF Chimera (version 1.15) as a graphical user interface on an Apple MacBook Pro (Retina, 13-inch, Mid-2014, equipped with a 2.8 GHz dual-core Intel Core i5 processor, 8 GB 1600 MHz DDR3 memory, Intel Iris 1536 MB graphics, and 500 GB Apple SSD SM0512F storage). The 3D crystal structure of the human *N*-methyl-D-aspartate (*h*NMDA) receptor (PDB ID: 7EU7) was downloaded from the Protein Databank (**https://www.rcsb.org**). Before the molecular docking process, the protein structure (PDB ID: 7EU7) was prepared using UCSF Chimera. The 2D structures of the synthesized (hetero)aryl amines and *N*-(hetero)aryl acetamides were generated using ChemBioDraw Ultra (version 14.0.0.117). Then, the conversion of the 2D skeletons to the related 3D structures of the ligands and their energy minimization processes (by the MM2 force field calculation method) was carried out using Chem3D Ultra (version 14.0.0.117). Also, structure editing steps (including dock prep and minimize structure) for the 3D ligands were repeated using UCSF Chimera. The 3D structures of medicinal compounds, which are shown in Fig. 8, were downloaded from PubChem (**https://pubchem.ncbi.nlm.nih.gov**). All the 3D structures of the mentioned medicinal compounds underwent the aforementioned structure editing steps using UCSF Chimera. All the protein–ligand interactions were analyzed using UCSF Chimera and BIOVIA Discovery Studio (version v21.1.0.20298). The 3D figures of the protein–ligand interactions were visualized using UCSF Chimera, and the related 2D projects were drawn using ChemBioDraw Ultra. The *in silico* ADME and toxicity analyses were investigated using SwissADME (**http://www.swissadme.ch**) and Deep-PK (**https://biosig.lab.uq.edu.au/deeppk/**), respectively.

4. Conclusions

In this paper, diverse green and efficient reaction strategies for the simple reduction (hydrogenation) and one-pot two-step reductive acetylation of nitro(hetero)arenes using a core–shell-type Fe_3O_4@APTMS@Cp_2ZrCl_x (x = 0, 1, 2) magnetically recoverable nanocomposite as a powerful nanocatalytic system have been reported. Notably, in the presented protocols, the as-prepared superparamagnetic Fe_3O_4@APTMS@Cp_2ZrCl_x (x = 0, 1, 2) nanocomposite had satisfactory turnover numbers (TONs) and turnover frequencies (TOFs) and also acceptable reusability. In this paper, the potential biological effect of the synthesized (hetero)aryl amines and *N*-(hetero)aryl acetamides, as a series of small organic molecules, against the transmembrane domain (TMD) of the human *N*-methyl-D-aspartate (*h*NMDA) receptor based on molecular docking studies has also been investigated. Besides, the drug-likeness properties of *N*-(3-(1-hydroxyethyl)phenyl)acetamide, as the hit compound, using *in silico* ADMET analyses, have been explored. Notably, research to find and develop new and green synthetic strategies for pharmaceutically interesting small organic molecules is underway in our research group.

Data availability

Data will be made available on request.

Conflicts of interest

The authors declare that they have no known competing financial interests or personal relationships that could have appeared to influence the work reported in this paper.

Acknowledgements

The authors gratefully appreciate the financial support of this work from the Research Council of Urmia University.

References

1 (*a*) D.-S. Zhang, Y. Liu, X. Ren, F. Geng, Y.-Z. Zhang, Y. Baikeli, M. Yang, Z. Liu, Y. Wang, X. Zhang and L. Geng, *Colloids Interface Sci. Commun.*, 2023, **56**, 100730; (*b*) M. Shahid, Z. H. Farooqi, R. Begum, M. Arif, W. Wu and A. Irfan, *Crit. Rev. Anal. Chem.*, 2020, **50**, 513–537; (*c*) P. Kovacic and R. Somanathan, *J. Appl. Toxicol.*, 2014, **34**, 810–824; (*d*) S. Sun, Z. Zhang, S. Li, J. Le, H. Qian, X. Yin, Y. Liu, W. Yang and Y. Chen, *J. Mater. Sci.*, 2023, **58**, 5587–5598; (*e*) S. Aghajani, M. Mohammadikish and M. Khalaji-Verjani, *Langmuir*, 2023, **39**, 8484–8493; (*f*) R. Sharma, P. S. Sagara, D. Sharma and A. Chaudhary, *J. Organomet. Chem.*, 2024, **1018**, 123294; (*g*) M. Mirhosseyni, G. Mohammadi Ziarani and A. Badiei, *J. Mol. Struct.*, 2025, **1321**, 139763; (*h*) M. Bakhtiarian, M. Safaei and M. M. Khodaei, *J. Mol. Struct.*, 2025, **1321**, 139913; (*i*) S. A. Haladu, K. A. Elsayed, A. A. Manda, T. S. Kayed, F. Ercan, S. M. Magami, S. Akhtar, A. ben Ahmed, M. A. Hafez and A. Elhassan, *J. Mol. Struct.*, 2025, **1321**,

139930; (*j*) M. Arif, A. Rauf, H. Raza, S. Ben Moussa, S. M. Haroon, A. Y. A. Alzahrani and T. Akhter, *Int. J. Biol. Macromol.*, 2024, **275**, 133633; (*k*) N. Y. Baran, M. Çalişkan, A. Özpala and T. Baran, *Int. J. Biol. Macromol.*, 2024, **262**, 130134; (*l*) C. C. Naik, D. P. Kamat and S. K. Gaonkar, *Int. J. Biol. Macromol.*, 2024, **286**, 131752; (*m*) A. Khalil, A. Khan, T. Kamal, A. A. P. Khan, S. B. Khan, M. T. S. Chani, K. A. Alzahrani and N. Ali, *Int. J. Biol. Macromol.*, 2024, **262**, 129986; (*n*) N. Y. Baran, *J. Organomet. Chem.*, 2024, **1008**, 123047; (*o*) R. Mondal, R. Ghanta, T. Chowdhury, A. Bhaumik and T. Chattopadhyay, *J. Mol. Struct.*, 2025, **1322**, 140287; (*p*) V. Aggarwal, E. Bala, S. Saima, S. Pathan, S. Guleria, S. Sharma, M. Selvaraj and P. K. Verma, *Synlett*, 2024, **35**, 245–267; (*q*) M. Mahendran, Y. Mariappan, R. Thamizhselvan and S. Vembu, *Mat. Adv.*, 2024, **5**, 3890–3903; (*r*) S. Iniyan, A. Vijayaprabhakaran, C. Sebastian and M. Kathiresan, *Mat. Adv.*, 2024, **5**, 7006–7015; (*s*) S. Taimur, S. Rehman, M. Ellahi, S. Rizwan, H. Razzaq and T. Yasin, *Mat. Adv.*, 2024, **5**, 9428–9444; (*t*) F. Eshrati, H. Ghafuri, P. Hanifehnejad and H. Dogari, *Mat. Adv.*, 2025, **6**, 278–297; (*u*) B.-B. Xing, Y.-S. Wang, T. Zhang, J.-Y. Liu, H. Jiao and L. Xu, *Mat. Adv.*, 2025, **3**, 756–765; (*v*) M. A. Pandit, D. S. H. Kumar, M. Varkolu and K. Muralidharan, *Nanoscale Adv.*, 2025, **7**, 1143–1153; (*w*) R. Mozafari, M. Mohammadi, S. Moradi and M. Ghadermazi, *RSC Adv.*, 2025, **15**, 1358–1374; (*x*) W. Guo, Y. Zheng, W. Xiang and Y. Zhang, *RSC Sustain.*, 2025, **3**, 243–254.

2 (*a*) M. C. Manjula, S. Manjunatha, K. L. Nagashree, M. Shivanna, M. P. Rao, N. Nanda and P. Ramachandra, *ChemistrySelect*, 2023, **8**, e202300936; (*b*) S. Sghajani and M. Mohammadikish, *Langmuir*, 2022, **38**, 8686–8695; (*c*) J. Song, Z.-F. Huang, L. Pan, K. Li, X. Zhang, L. Wang and J.-J. Zou, *Appl. Catal. B Environ.*, 2018, **227**, 386–408; (*d*) S. Kumar and S. K. Maurya, *J. Org. Chem.*, 2023, **88**, 8690–8702; (*e*) X. Li, J. An, Z. Gao, C. Xu, Y. Cheng, S. Li, L. Li and B. Tang, *Chem. Sci.*, 2023, **14**, 3554–3561; (*f*) S. Karimi, M. Gholinejad, R. Khezri, J. M. Sansano, C. Nájera and M. Yus, *RSC Adv.*, 2023, **13**, 8101–8113; (*g*) H. Jiang, G. Yuan, Z. Cui, Z. Zhao, Z. Dong, J. Zhang, Y. Cong and X. Li, *Ind. Eng. Chem. Res.*, 2023, **62**, 13355–13367; (*h*) H. Yu, J. Liu, Q. Wan, G. Zhao, E. Gao, J. Wang, B. Xu, G. Zhao and X. Fan, *Mol. Catal.*, 2023, **540**, 113045; (*i*) Z. Ma, J. Chen, M. Chen, L. Dong, W. Mao, Y. Long and J. Ma, *Mol. Catal.*, 2023, **547**, 113372; (*j*) S. Taheri, M. M. Heravi and A. Saljooqi, *Sci. Rep.*, 2023, **13**, 17566; (*k*) A. Maurya, U. K. Patel, S. Kumar and A. Agarwal, *RSC Adv.*, 2024, **14**, 29505–29517; (*l*) F. Doraghi, Y. Mohammadkhani Kalooei, N. Mehdi Zadeh Darban, B. Larijani and M. Mahdavi, *J. Organomet. Chem.*, 2024, **1019**, 123313; (*m*) P. Ding, E. Fayad, O. A. A. Ali and H.-L. Qin, *Tetrahedron*, 2024, **167**, 134269; (*n*) C. A. Romero-Soto, A. L. Iglesias, A. F. Velázquez-Ham, J. P. Camarena-Díaz, E. Correa-Ayala, J. L. Gomez-Lopez, D. Chávez, A. Ochoa-Terán, G. Aguirre, A. L. Rheingold, D. B. Grotjahn, M. Parra-Hake and V. Miranda-Soto, *RSC Adv.*, 2024, **14**, 24019–24030; (*o*) Y. Wei, S. Wang, Y. Zhang, M. Li, J. Hu, Y. Liu, J. Li, L. Yu, R. Huang and D. Deng, *ACS Catal.*, 2023, **13**, 15824–15832; (*p*) J. Wu, W. Lang, H. Li, K. Du, J. Deng, S. Zhao, W. Zhang, Z. Peng and Z. Liu, *ACS Sustainable Chem. Eng.*, 2023, **11**, 14960–14968; (*q*) J. Ma, X. Mao, C. Hu, X. Wang, W. Gong, D. Liu, R. Long, A. Du, H. Zhao and Y. Xiong, *J. Am. Chem. Soc.*, 2024, **146**, 970–978; (*r*) A. Singh, O. Singh, A. Maji, S. Singh, N. Singh, P. K. Maji and K. Ghosh, *Mol. Catal.*, 2024, **555**, 113835; (*s*) W. Gao, Y. Gao, B. Liu, J. Kang, Z. Zhang, M. Zhang and Y. Zou, *RSC Adv.*, 2024, **14**, 5055–5060; (*t*) Z. Kefayati, M. Malmir and M. M. Heravi, *Res. Chem. Intermed.*, 2024, **50**, 127–146; (*u*) A. S. Hazari, M. L. Frisch, Y. Wen, M. D. Stankovic and C. P. Berlinguette, *J. Am. Chem. Soc.*, 2024, **146**, 28153–29160; (*v*) X. Zhuang, H. Song, J. Wang, Z. Zhang, J. Wang, B. Sun, W. Su and C. Jin, *Green Chem.*, 2024, **26**, 9682–9689.

3 (*a*) J. B. Zimmerman, P. T. Anastas, H. C. Erythropel and W. Leitner, *Science*, 2020, **367**, 397–400; (*b*) H. C. Erythropel, J. B. Zimmerman, T. M. de Winter, L. Petitjean, F. Melnikov, C. H. Lam, A. W. Lounsbury, K. E. Mellor, N. Z. Janković, Q. Tu, L. N. Pincus, M. M. Falinski, W. Shi, P. Coish, D. L. Plata and P. T. Anastas, *Green Chem.*, 2018, **20**, 1929–1961; (*c*) T. Keijer, V. Bakker and J. C. Slootweg, *Nat. Chem.*, 2019, **11**, 190–195; (*d*) P. Anastas and N. Eghbali, *Chem. Soc. Rev.*, 2010, **39**, 301–312; (*e*) H. Mousavi, *Int. J. Biol. Macromol.*, 2021, **186**, 1003–1166; (*f*) M. Rimaz, Z. Jalalian, H. Mousavi and R. H. Prager, *Tetrahedron Lett.*, 2016, **57**, 105–109; (*g*) M. Rimaz, J. Khalafy and H. Mousavi, *Res. Chem. Intermed.*, 2016, **42**, 8185–8200; (*h*) A. s. Alqahtani and S. Elbeltagi, *J. Organomet. Chem.*, 2025, **1027**, 123508; (*i*) S. Swami, N. Sharma, G. Sharma and R. Shrivastava, *RSC Adv.*, 2025, **15**, 2361–2415; (*j*) N. Hassanzadeh, M. G. Dekamin and E. Valiey, *Nanoscale Adv.*, 2025, **7**, 99–123.

4 (*a*) L. Peng, Y. Zhao, T. Yang, Z. Tong, Z. Tang, A. Orita and R. Qiu, *Top. Curr. Chem.*, 2022, **380**, 44; (*b*) L.-P. Mo and Z.-H. Zhang, *Curr. Org. Chem.*, 2011, **15**, 3800–3823; (*c*) K. Nikoofar and Z. Khademi, *Res. Chem. Intermed.*, 2016, **42**, 3929–3977; (*d*) N. Suzuki, S. Ito, M. Kawate and T. Takemoto, *J. Organomet. Chem.*, 2023, **1001**, 122883; (*e*) J. Okuda, *J. Organomet. Chem.*, 2023, **1000**, 122833; (*f*) M. Chegeni and M. Mehri, *J. Organomet. Chem.*, 2023, **984**, 122585; (*g*) W. Asim, A. S. Waheeb, M. A. Awad, A. M. Kadhum, A. Ali, S. H. Mallah, M. A. Iqbal and M. M. Kadhim, *J. Mol. Struct.*, 2022, **1250**, 131925; (*h*) N. Moeini, M. Ghadermarzi and S. Molaei, *J. Mol. Struct.*, 2022, **1251**, 131982; (*i*) H. Maati, O. Amadine, Y. Essamlali, B. Rezki, I. Ayouch, H. Mahi, K. Abdelouahdi and M. Zahouily, *J. Mol. Struct.*, 2023, **1294**, 136347; (*j*) A. S. Al-Wasidi, *J. Organomet. Chem.*, 2024, **1022**, 123403; (*k*) L. K. Dilmukhametova, M. G. Shaibakova and I. R. Ramazanov, *Russ. Chem. Bull.*, 2024, **73**, 1894–1899; (*l*) M. Rimaz, J. Khalafy, H. Mousavi, S. Bohlooli and B. Khalili, *J. Heterocycl. Chem.*, 2017, **54**, 3174–3186; (*m*) M. Rimaz, H. Mousavi, P. Keshavarz and B. Khalili, *Curr. Chem. Lett.*, 2015, **4**, 159–168; (*n*) M. Rimaz, H. Mousavi, M. Behnam and B. Khalili, *Curr. Chem. Lett.*, 2016, **5**, 145–154; (*o*) M. Rimaz, H. Mousavi, B. Khalili and L. Sarvari, *J.*

Iran. Chem. Soc., 2019, **16**, 1687–1701; (*p*) M. Rimaz, H. Mousavi, B. Khalili and F. Aali, *J. Chin. Chem. Soc.*, 2018, **65**, 1389–1397; (*q*) S.-J. Yao, J.-M. Lin, L.-Z. Dong, Y.-L. Li, N. Li, J. Li and Y.-Q. Lan, *Sci. Bull.*, 2024, **69**, 1418–1426; (*r*) A. S. Al-Wasidi, *J. Organomet. Chem.*, 2025, **1022**, 123403; (*s*) J. Wu, M. Yang, D. Leng, Q. Hu, Y. Yao, H. Sun and Z. Gao, *RSC Adv.*, 2025, **15**, 1747–1753.

5 D. Wang and D. Astruc, *Chem. Soc. Rev.*, 2017, **46**, 816–854.

6 M. Bystrzanowska, P. Petkov and M. Tobiszewski, *ACS Sustainable Chem. Eng.*, 2019, **7**, 18434–18443.

7 (*a*) D. Wang and D. Astruc, *Chem. Rev.*, 2014, **114**, 6949–6985; (*b*) M. G. Sibi, D. Verma and J. Kim, *Catal. Rev.*, 2020, **62**, 163–311; (*c*) Q. Sun, X.-Q. Zhang, Y. Wang and A.-H. Lu, *Chin. J. Catal.*, 2015, **36**, 683–691; (*d*) M. B. Gawande, A. Goswami, T. Asefa, H. Guo, A. V. Biradar, D.-L. Peng, R. Zboril and R. S. Varma, *Chem. Soc. Rev.*, 2015, **44**, 7540–7590; (*e*) B. Zuo, W. Li, X. Wu, S. Wang, Q. Deng and M. Huang, *Chem.–Asian J.*, 2020, **15**, 1248–1265; (*f*) Z. Li, M. Li, Z. Bian, Y. Kathiraser and S. Kawi, *Appl. Catal. B Environ.*, 2016, **188**, 324–341; (*g*) H. Veisi, M. Pirhayati, P. Mohammadi, T. Tamoradi, S. Hemmati and B. Karmakar, *RSC Adv.*, 2023, **13**, 20530–20556; (*h*) N. Kaviani, S. Behrouz, A. A. Jafari and M. N. Soltani Rad, *RSC Adv.*, 2023, **13**, 30293–30305; (*i*) M. Mohammadi, A. Ghorbani-Choghamarani and S. M. Ramish, *J. Mol. Struct.*, 2023, **1292**, 136115; (*j*) M. Y. Saleh, A. K. O. Aldulaimi, S. M. Saeed and A. H. Adhab, *J. Mol. Struct.*, 2025, **1321**, 139597; (*k*) D. Singh, A. Kumar, Y. Jadeja, S. V. Menon, P. Singh, S. M. Ibrahim, M. Singh, M. K. Abosaoda, S. B. AlReshaidan and M. A. El-Meligy, *J. Mol. Struct.*, 2025, **1321**, 140133; (*l*) H. V. Le, H. X. Le, V. T. B. Nguyen, T. T. Le, H. N. Nguyen, T. T. H. Nguyen, T. T. Nguyen, P. H. Ho, K. D. Nguyen and D. P. Tran, *ChemistrySelect*, 2024, **9**, e202402007; (*m*) Y. Wang, X. Wang, Y. Dong, M. Peng, L. Guo, M. Cui, Y. He, J. Yi, H. Ma, H. Zhang and H. Fan, *Green Chem.*, 2024, **26**, 6131–6138; (*n*) H. P Mata, J. M. Anghinoni, E. C. Silva, P. Macchion, S. S. Ferreira, J. F. de Souza, E. J. Lenardão and A. R. Fajardo, *J. Organomet. Chem.*, 2025, **1025**, 123478; (*o*) M.-S. Mashhoori and R. Sandaroos, *J. Organomet. Chem.*, 2025, **1025**, 123486; (*p*) Q. Qiu, J. R. Song, H. Zheng, M. Shahriari, A. F. El-kott, A. G. Alkhathami and K. Morcy, *J. Organomet. Chem.*, 2025, **1023**, 123423; (*q*) K. Dolatyari and M. M. Khodaei, *J. Organomet. Chem.*, 2024, **1021**, 123352; (*r*) L. Bhosale, R. Gurav, A. Gurav, S. Sankpal and S. Hangirgekar, *J. Organomet. Chem.*, 2024, **1021**, 123341; (*s*) H. Jia, Y. Cui, X. Yuan, Y. Xu and Y. Li, *J. Organomet. Chem.*, 2024, **1021**, 123354.

8 (*a*) C. Capello, U. Fischer and K. Hungerbühler, *Green Chem.*, 2007, **9**, 927–934; (*b*) D. Prat, J. Hayler and A. Wells, *Green Chem.*, 2014, **16**, 4546–4551; (*c*) V. Hessel, N. N. Tran, M. R. Asrami, Q. D. Tran, N. V. C. Long, M. Escribà-Gelonch, J. O. Tejada, S. Linke and K. Sunmacher, *Green Chem.*, 2022, **24**, 410–437; (*d*) C. J. Clarke, W.-C. Tu, O. Levers, A. Bröhl and J. P. Hallett, *Chem. Rev.*, 2018, **118**, 747–800; (*e*) F. P. Byrne, S. Jin, G. Paggiola, T. H. M. Petchey, J. H. Clarck, T. J. Farmer, A. J. Hunt, C. R. McElory and J. Sherwood, *Sustainable Chem. Processes*, 2016, **4**, 7; (*f*) R. N. Butler and A. C. Coyne, *Chem. Rev.*, 2010, **110**, 6302–6337; (*g*) A. Chanda and V. V. Fokin, *Chem. Rev.*, 2009, **109**, 725–748; (*h*) M.-O. Simon and C.-J. Li, *Chem. Soc. Rev.*, 2012, **41**, 1415–1427.

9 (*a*) R. Tenchov, J. M. Sasso and Q. A. Zhou, *ACS Chem. Neurosci.*, 2024, **15**, 2665–2694; (*b*) K. Singh, A. Kaur, B. Goyal and D. Goyal, *ACS Chem. Neurosci.*, 2024, **15**, 2545–2564; (*c*) M. Farzan, B. Abedi, I. Bhia, A. Madanipour, M. Farzan, M. Bhia, A. Aghaei, I. Kheirollahi, M. Motallebi, H. Amini-Khoei and Y. Nuri Ertas, *ACS Chem. Neurosci.*, 2024, **15**, 2966–2981; (*d*) S. Willems, D. Zaienne and D. Merk, *J. Med. Chem.*, 2021, **64**, 9592–9638; (*e*) O. Hansson, *Nat. Med.*, 2021, **27**, 954–963; (*f*) D. M. Wilson, M. R. Cookson, L. Van Den Bosch, H. Zetterberg, D. M. Holtzman and I. Dewachter, *Cell*, 2023, **186**, 693–714; (*g*) J. Wang, Y. Cao, Y. Lu, H. Zhu, J. Zhang, J. Che, R. Zhuang and J. Shao, *Eur. J. Med. Chem.*, 2024, **264**, 115998; (*h*) Q. Li, Q. Liao, S. Qi, H. Huang, S. He, W. Lyu, J. Liang, H. Qin, Z. Cheng, F. Yu, X. Dong, Z. Wang, L. Han and Y. Han, *Eur. J. Med. Chem.*, 2024, **271**, 116386; (*i*) Z. Cai, Z. Yang, H. Li and Y. Fang, *Bioorg. Chem.*, 2024, **147**, 107386; (*j*) J. Zhang, P. Jiang, S. Wang, M. Li, Z. Hao, W. Guan, J. Pan, J. Wu, Y. Zhang, H. Li, L. Chen, B. Yang and Y. Liu, *Bioorg. Chem.*, 2024, **153**, 107819.

10 (*a*) T.-S. Chou, M. Epstein, R. G. Fritzemeier, N. S. Akins, S. Paladugu, E. Z. Ullman, D. C. Liotta, S. F. Traynelis and H. Furukawa, *Nature*, 2024, **632**, 209–217; (*b*) K. Michalski and H. Furukawa, *Sci. Adv.*, 2024, **10**, eadl5952; (*c*) C. Geoffroy, R. Berraud-Pache, N. Chéron, I. McCort-Tranchepain, J. Doria, P. Paoletti and L. Mony, *ACS Chem. Neurosci.*, 2024, **15**, 3321–3343; (*d*) Y. Zhang, F. Ye, T. Zhang, S. Lv, L. Zhou, D. Du, H. Lin, F. Guo, C. Luo and S. Zhu, *Nature*, 2021, **596**, 301–305; (*e*) M. R. Wilcox, A. Nigam, N. G. Glasgow, C. Narangoda, M. B. Phillips, D. S. Patel, S. Mesbahi-Vasey, A. L. Turcu, S. Vázquez, M. G. Kurnikova and J. W. Johnson, *Nat. Commun.*, 2022, **13**, 4114; (*f*) A. Camargo, A. P. Dalmagro, G. A. Altê, A. L. B. Zeni, C. I. Tasca and A. L. S. Rodrigues, *Chem. Biol. Interact.*, 2023, **375**, 110440; (*g*) P. Song, C. Ma, S. Wang, Y. Zhang, L. Xu, F. Fang, X. Huang, Y. Zhang, Q. Mao, C. Shi, M. Cheng and Y. Xu, *Bioorg. Med. Chem.*, 2025, **119**, 118063; (*h*) Z. Wang, Y. He, G. Chen and X. Bao, *New J. Chem.*, 2025, **49**, 2319–2334.

11 H. Mousavi, M. Rimaz and B. Zeynizadeh, *ACS Chem. Neurosci.*, 2024, **15**, 1828–1881.

12 (*a*) V. T. Sabe, T. Ntombela, L. A. Jhamba, G. E. M. Maguire, T. Govender, T. Naicker and H. G. Kruger, *Eur. J. Med. Chem.*, 2021, **224**, 113705; (*b*) P. B. Cox and R. Gupta, *ACS Med. Chem. Lett.*, 2022, **13**, 1016–1029; (*c*) A. Tirehdast, S. Sheikhi-Mohammareh, H. Sabet-Sarvestani, M. G. Organ, V. Semeniuchenko and A. Shiri, *RSC Adv.*, 2024, **14**, 29122–29133; (*d*) H. Mousavi, B. Zeynizadeh and M. Rimaz, *Bioorg. Chem.*, 2023, **135**, 106390; (*e*) D. E. Arthur, *Inform. Med. Unlocked*, 2023, **41**, 101301; (*f*) N. H. Siddiquee, M. I. Hossain, M. E. K. Talukder, S. A. A. Nirob, M. Shourav, I. Jahan, U. H. A. Tamanna, P. Das, R. Akter, M. hasan, M. Abdullah-Al-Mamun and O. Saha, *Inform. Med. Unlocked*, 2023, **45**, 101458; (*g*) S. S. Marufa, T. Rahman, M. M. Rahman, M. Rahman,

S. J. Khan, R. Jahan, H. Nishino, M. S. Alam and A. Haque, *RSC Adv.*, 2024, **14**, 35198–35214.

13 (*a*) H. Mousavi, B. Zeynizadeh and M. Hasanpour Galehban, *Nanoscale Adv.*, 2024, **6**, 3961–3977; (*b*) M. Hasanpour Galehban, B. Zeynizadeh and H. Mousavi, *J. Mol. Struct.*, 2023, **1271**, 134017; (*c*) M. Hasanpour Galehban, B. Zeynizadeh and H. Mousavi, *RSC Adv.*, 2022, **12**, 16454–16478; (*d*) M. Hasanpour Galehban, B. Zeynizadeh and H. Mousavi, *RSC Adv.*, 2022, **12**, 11164–11189; (*e*) B. Zeynizadeh, H. Mousavi and F. Mohammad Aminzadeh, *J. Mol. Struct.*, 2022, **1255**, 131926; (*f*) B. Zeynizadeh, F. Mohammad Aminzadeh and H. Mousavi, *Res. Chem. Intermed.*, 2021, **47**, 3289–3312; (*g*) R. Bakhshi, B. Zeynizadeh and H. Mousavi, *J. Chin. Chem. Soc.*, 2020, **67**, 623–637; (*h*) B. Zeynizadeh, H. Mousavi and S. Zarrin, *J. Chin. Chem. Soc.*, 2019, **66**, 928–933; (*i*) B. Zeynizadeh, F. Mohammad Aminzadeh and H. Mousavi, *Res. Chem. Intermed.*, 2019, **45**, 3329–3357; (*j*) B. Zeynizadeh, F. Mohammad Aminzadeh and H. Mousavi, *Green Process. Synth.*, 2019, **8**, 742–755; (*k*) B. Zeynizadeh, R. Younesi and H. Mousavi, *Res. Chem. Intermed.*, 2018, **44**, 7331–7352; (*l*) H. Mousavi, B. Zeynizadeh, R. Younesi and M. Esmati, *Aust. J. Chem.*, 2018, **71**, 595–609.

14 B. Zeynizadeh and F. Sepehraddin, *J. Iran. Chem. Soc.*, 2017, **14**, 2649–2657.

15 B. Zeynizadeh, F. Sepehraddin and H. Mousavi, *Ind. Eng. Chem. Res.*, 2019, **58**, 16379–16388.

16 B. Zeynizadeh, H. Mousavi and F. Sepehraddin, *Res. Chem. Intermed.*, 2020, **46**, 3361–3382.

17 (*a*) H. K. Kadam and S. G. Tilve, *RSC Adv.*, 2015, **5**, 83391–83470; (*b*) A. Mannu, A. Grabulosa and S. Baldino, *Catalysts*, 2020, **10**, 162; (*c*) H. M. Marçon and J. C. Pastre, *RSC Adv.*, 2022, **12**, 7980–7989; (*d*) J. Song, M. Hua, X. Huang, A. Visa, T. Wu, H. Fan, M. Hou, Z. Zhang and B. Han, *Green Chem.*, 2021, **23**, 1259–1265; (*e*) C. A. Akinnawo, N. Bingwa and R. Meijboom, *New J. Chem.*, 2021, **45**, 7878–7892; (*f*) J. Song, B. Zhou, H. Zhou, L. Wu, Q. Meng, Z. Liu and B. Han, *Angew. Chem., Int. Ed.*, 2015, **54**, 9399–9403; (*g*) T. Wang, H. Xu, J. Hu and Y. Zhang, *New J. Chem.*, 2020, **44**, 14686–14694; (*h*) Z. Wang, C. Xie, X. Li, J. Nie, H. Yang and Z. Zhang, *Chem. Commun.*, 2022, **58**, 4067–4070; (*i*) Y. Sha, Z. Xiao, H. Zhou, K. Yang, Y. Song, N. Li, R. He, K. Zhi and Q. Liu, *Green Chem.*, 2017, **19**, 4829–4837; (*j*) Y. Wang, J. Huang, S. Lu, P. Li, X. Xia, C. Li and F. Li, *New J. Chem.*, 2020, **44**, 20308–20315; (*k*) T. Wang, A. Hu, G. Xu, C. Liu, H. Wang and Y. Xia, *Catal. Lett.*, 2019, **149**, 1845–1855; (*l*) L. Ye, Y. Han, Z. Yu, M. Zhang, J. Xiong, R. Zhang, X. Li, Y. Qiao and X. Lu, *Fuel*, 2022, **328**, 125233; (*m*) Y. Zhang, X. Shen, L. Hu, Z. Wu, X. Wang and J. Jiang, *Biomass Convers. Biorefin.*, 2024, **14**, 2045–2061; (*n*) Q. Peng, H. Wang and Y. Xia, *Catal. Lett.*, 2023, **153**, 720–731; (*o*) Q. Peng, X. Li, X. Wang, Y. Li, Y. Xia, X. Liu and H. Wang, *Sustain. Energy Fuels*, 2021, **5**, 4069–4079; (*p*) G. Deshmukh and R. Murugavel, *Synlett*, 2025, **36**, 75–81; (*q*) H. Zarei, S. Sobhani and J. M. Sansano, *Appl. Organomet. Chem.*, 2024, **38**, e7740; (*r*) S. Ma, X. Wang, J. Cao, H. Chen, Y. Lu and R. Wang, *ChemistrySelect*, 2024, **9**, e202400730; (*s*) S. Pachisia, R. Kishan, S. Yadav and R. Gupta, *Inorg. Chem.*, 2021, **60**, 2009–2022; (*t*) O. A. Luongo, M. Lemmerer, S. L. Albers and J. Streuff, *Angew. Chem., Int. Ed.*, 2024, **63**, e202413182.

18 (*a*) P. Patinl, Q. Zheng, K. Kurpiewsk and A. Dömling, *Nat. Commun.*, 2023, **14**, 5807; (*b*) A. Darvishi, H. Bakhshi and A. Heydari, *RSC Adv.*, 2022, **12**, 16535–16543; (*c*) E. Valeur and M. Bradley, *Chem. Soc. Rev.*, 2009, **38**, 606–631; (*d*) V. R. Pattabiraman and J. W. Bode, *Nature*, 2011, **480**, 471–479; (*e*) S. Kumari, A. V. Carmona, A. K. Tiwari and P. C. Trippier, *J. Med. Chem.*, 2020, **63**, 12290–12358; (*f*) S. S. R. Gupta, A. V. Nakhate, G. P. Deshmukh, S. Periasamy, P. S. Samudrala, S. K. Bhargava and M. L. Kantam, *ChemistrySelect*, 2018, **3**, 8436–8443; (*g*) M. Lubberink, W. Finnigan and S. L. Flitsch, *Green Chem.*, 2023, **25**, 2958–2970; (*h*) Y. Ge, W. Huang, S. Ahrens, A. Spannenberg, R. Jackstell and M. Beller, *Nat. Synth.*, 2024, **3**, 202–213; (*i*) Q. Yan, Q.-J. Yuan, A. Shatskiy, G. R. Alvey, E. V. Stepanova, J.-Q. Liu, M. D. Kärkäs and X.-S. Wang, *Org. Lett.*, 2024, **26**, 3380–3385.

19 (*a*) B. H. Rostein, S. Zaretsky, V. Rai and A. K. Yudin, *Chem. Rev.*, 2014, **114**, 8323–8359; (*b*) A. Dömling, W. Wang and K. Wang, *Chem. Rev.*, 2014, **112**, 3083–3135; (*c*) F. Sutanto, S. Shaabani, C. G. Neochoritis, T. Zarganes-Tzitzikas, P. Patil, E. Ghonchepour and A. Dömling, *Sci. Adv.*, 2021, **7**, eabd9307; (*d*) D. Hurtado-Rodríguez, A. Salinas-Torres, H. Rojas, D. Becerra and J.-C. Castillo, *RSC Adv.*, 2022, **12**, 35158–35176; (*e*) H. R. Chaudhary and D. M. Patel, *RSC Adv.*, 2024, **14**, 31072–31116; (*f*) C. Zavarise, J.-C. Cintrat, E. Romero and A. Sallustrau, *RSC Adv.*, 2024, **14**, 39253–39267; (*g*) M. Rimaz, H. Mousavi, M. Behnam, L. Sarvari and B. Khalili, *Curr. Chem. Lett.*, 2017, **6**, 55–68; (*h*) M. Rimaz, B. Khalili, G. Khatyal, H. Mousavi and F. Aali, *Aust. J. Chem.*, 2017, **70**, 1274–1284; (*i*) M. Rimaz, H. Mousavi, L. Nikpey and B. Khalili, *Res. Chem. Intermed.*, 2017, **43**, 3925–3937; (*j*) M. Rimaz, H. Mousavi, L. Ozzar and B. Khalili, *Res. Chem. Intermed.*, 2019, **45**, 2673–2694; (*k*) D. Zeleke and T. Damena, *Res. Chem.*, 2024, **7**, 101283; (*l*) N. Yaghmaeiyan, M. Mirzaei and A. Bamoniri, *Res. Chem.*, 2023, **5**, 100696; (*m*) S. Handique and P. Sharma, *Res. Chem.*, 2023, **5**, 100781; (*n*) S. S. Bhalodiya, M. P. Parmar, D. B. Upadhyay, C. D. Patel, D. P. Vala, D. Rajani and H. M. Patel, *Res. Chem.*, 2024, **7**, 101304; (*o*) M. Rimaz and H. Mousavi, *Turk. J. Chem.*, 2013, **37**, 252–261; (*p*) M. Behrouzi, K. Rabiei and S. Ghasemzadeh, *J. Organomet. Chem.*, 2024, **1022**, 123413; (*q*) F. Pirani and H. Eshghi, *J. Organomet. Chem.*, 2024, **1020**, 123339; (*r*) M. Tandi, V. Sharma, B. Gopal and S. Sundriyal, *RSC Adv.*, 2025, **15**, 1447–1489.

20 C. Sharma, A. K. Srivastava, A. Soni, S. Kumari and R. K. Joshi, *RSC Adv.*, 2020, **10**, 32516–32521.

21 V. S. Sypu, M. Bhaumik, K. Raju and A. Maity, *J. Colloid Interface Sci.*, 2021, **581**, 979–989.

22 S. Yang, Z.-H. Zhang, Q. Chen, M.-Y. He and L. Wang, *Appl. Organomet. Chem.*, 2018, **32**, e4132.

23 M. Pashaei and E. Mehdipour, *Appl. Organomet. Chem.*, 2018, **32**, e4226.
24 M. Piri, M. M. Heravi, A. Elhampour and F. Nemati, *J. Mol. Struct.*, 2021, **1242**, 130646.
25 A. K. Srivastava, H. Khandaka and R. K. Joshi, *SynOpen*, 2023, **7**, 121–129.
26 Z. Moradi and A. Ghorbani-Choghamarani, *Sci. Rep.*, 2023, **13**, 7645.
27 N. Seyedi, F. Shirini and H. Tajik, *J. Mol. Struct.*, 2023, **1285**, 135547.
28 M. Dabiri, A. Mnachekanian Salmasi, N. Salarinejad and S. Kazemi Movahed, *J. Mol. Struct.*, 2023, **1287**, 135609.
29 P. Mohammadi, M. M. Heravi, L. Mohammadi and A. Saljooqi, *Sci. Rep.*, 2023, **13**, 17375.
30 M. Z. Sarker, M. M. Rahman, H. Minami, M. S. I. Sarker and H. Ahmad, *Colloids Surf. A Physicochem. Eng. Asp.*, 2023, **668**, 131447.
31 M. Bayzidi and B. Zeynizadeh, *RSC Adv.*, 2022, **12**, 15020–15037.
32 A. Capperucci, M. Clemente, A. Cenni and D. Tanini, *ChemSusChem*, 2023, **16**, e202300086.
33 F. Dadvar and D. Elhamifar, *Nanoscale Adv.*, 2024, **6**, 5398–5408.
34 F. Gholamrezaei, S. Y. Ebrahimipour and E. Ghonchepour, *J. Organomet. Chem.*, 2024, **1019**, 123314.
35 B. Kaboudin, B. Burunli, M. Nazerian, T. Zhang and Y. Gu, *J. Organomet. Chem.*, 2025, **1025**, 123477.
36 V. Bilakanti, N. Gutta, V. K. Velisoju, M. Dumpalapally, S. Inkollu, N. Nama and V. Akula, *React. Kinet. Mech. Catal.*, 2020, **130**, 347–362.
37 N. K. Lamba, P. Choudhary, Twinkle, J. Kaushik, S. K. Choudhary and S. K. Sonkar, *Langmuir*, 2024, **40**, 18961–18967.
38 (*a*) H. van de Waterbeemd and E. Gifford, *Nat. Rev. Drug Discov.*, 2003, **2**, 192–204; (*b*) E. V. Feinberg, E. Joshi, V. S. Pande and A. C. Cheng, *J. Med. Chem.*, 2020, **63**, 8835–8848; (*c*) C.-Y. Jia, G.-F. Hao and G.-F. Yang, *Drug Discov. Today*, 2020, **25**, 248–258; (*d*) L. L. G. Ferreira and A. D. Andricopulo, *Drug Discov. Today*, 2019, **24**, 1157–1165; (*e*) L. Guan, H. Yang, Y. Cai, L. Sun, P. Di, W. Li, G. Liu and Y. Tang, *Med. Chem. Commun.*, 2019, **10**, 148–157; (*f*) S. Q. Pantaleão, P. O. Fernandes, J. E. Gonçalves, V. G. Maltarollo and K. M. Honorio, *ChemMedChem*, 2022, **17**, e202100542; (*g*) R. Sayad, A. Bouzina, Y. O. Bouone, D. Beldjezzia, A. Djemel, M. Ibrahim-Ouali, N.-E. Aouf and Z. Aouf, *RSC Adv.*, 2024, **14**, 24585–24603; (*h*) A. Bouzina, Y. O. Bouone, O. Sekiou, M. Aissaoui, T.-S. Ouk, A. Djemel, R. Mansouri, M. Ibrahim-Ouali, Z. Bouslama and N.-E. Aouf, *RSC Adv.*, 2023, **13**, 19567–19584; (*i*) S. S. Ramasamy, K. Adhigaman, V. Nandakumar, A. Sundarasamy, S. Jagadeesan, M. Saravanakumar, J. G. Malecki, N. Easwaran and S. Thangaraj, *J. Mol. Struct.*, 2025, **1321**, 140218.
39 (*a*) A. Daina, O. Michielin and V. Zoete, *Sci. Rep.*, 2017, **7**, 42717; (*b*) B. Bakchi, A. D. Krishna, E. Sreecharan, V. B. J. Ganesh, M. Niharika, S. Maharshi, S. B. Puttagunta, D. K. Sigalapalli, R. R. Bhandare and A. B. Shaik, *J. Mol. Struct.*, 2022, **1259**, 132712.
40 Y. Myung, A. G. C. de Sá and D. B. Ascher, *Nucleic Acids Res.*, 2024, **52**, W469–W475.